



**Politecnico
di Torino**

Politecnico di Torino

Master of Science in
Automotive Engineering
A.y. 2021/2022
October 2022

**Effect of using Additive
Manufacturing substrates on
fatigue performance of adhesively
bonded joints**

Advisors:
Prof. Luca Goglio
Prof. Sayed Nassar

Candidate:
Camilla Salvatore

© Copyright by Camilla Salvatore, 2022

All rights reserved

To my parents, for your constant love and support

To my best friends

Ad maiora!

ACKNOWLEDGMENTS

Firstly, I would like to express my deepest gratitude to my Thesis advisors, Dr. Sayed Nassar and Professor Luca Goglio, who guided me throughout this work, showing me continuous support. Then I would like to thank and express my appreciation to whoever has participated in this research, starting from my head-tutors from Stellantis S.P.A.. A special thanks to Maura Fontana, for her patience, guidance and support. Having always a nice word, she helped me to believe in myself even in the most difficult and challenging moments. Her advices and assistance, even if by remote, made my work a lot easier. Then, I would like to acknowledge Stefano Slaghenaufi for providing me his valuable recommendations regarding this study, with great professionalism. Moreover, I would like to deeply thank Dr. Marco Gerini Romagnoli, who helped me for several months with all the activities I have done at FAJRI and taught me with great passion how to deal with adhesive bonding. His presence and his precious suggestions have been fundamental for my experience in the United States. Last but not least, a special mention is needed for Daniel Nappi: part of my research is a continuation of his study and he always gave me the right advice during this journey. But above all, I would like to thank him for his unconventional way to make me a better version of myself.

Camilla Salvatore

ABSTRACT

EFFECT OF USING ADDITIVE MANUFACTURING SUBSTRATES ON FATIGUE PERFORMANCE OF ADHESIVELY BONDED JOINTS

by

Camilla Salvatore

Adviser: Prof. Luca Goglio

This research investigates on the influence of substrate manufacturing method on the fatigue performance of adhesively bonded joints. High cycle fatigue tests are conducted on two configurations of SLJs. The substrates are made of 17-4 PH stainless steel. Additive Manufactured substrates are compared to wrought substrates. Fatigue tests are carried out at constant stress amplitude for two levels of mean stress. The effect of the mean stress is discussed.

The effect of stress ratio and material manufacturing of DLJs in fatigue lap shear tests is discussed. The substrates are made of AlSi10Mg aluminum alloy. The test samples are bonded using a new single-part epoxy adhesive. A FE model is used to characterize the adhesive. The aim is to obtain a reliable model able to simulate real life mechanical behavior of complex bonded joints configurations and find a methodology for adhesive fatigue life prediction. Virtual results are compared with experimental data.

TABLE OF CONTENTS

ACKNOWLEDGMENTS	iv
ABSTRACT	v
LIST OF TABLES	viii
LIST OF FIGURES	ix
NOMENCLATURE	xv
CHAPTER ONE	
INTRODUCTION	1
1.1 Introduction	1
1.2 Literature survey	6
1.3 Objectives	9
CHAPTER TWO	
EXPERIMENTAL SETUP AND TEST PROCEDURE	11
2.1 Experimental procedure	11
2.2 Single Lap Joint Test	18
2.2.1 Joint Geometry	18
2.2.2 Bonding Process	21
2.2.3 Quasi-static Shear-Tensile Tests	24
2.2.4 Fatigue Shear-Tensile Tests	24
CHAPTER THREE	
FINITE ELEMENT MODELS	32
3.1 Finite Element Modeling	32
3.2 Double Lap Joints	33
3.2.1 Cohesive Zone Modeling	39
3.3 Linear Elastic Elements	44

TABLE OF CONTENTS - Continued

CHAPTER FOUR	
METHODOLOGY FOR FATIGUE LIFE PREDICTION	45
4.1 Procedure in nCode Design Life	45
4.1.1 Material properties and parameters	47
4.2 Mesh sensitivity analysis	49
CHAPTER FIVE	
RESULTS AND DISCUSSIONS	50
5.1 Experimental testing results	51
5.1.1 Single Lap Joints	51
5.1.1.1 Effect of material manufacturing	53
5.1.1.2 Effect of the Average Surface Roughness	58
5.1.2 Double Lap Joints	66
5.1.2.1 Static Results	66
5.1.2.2 Fatigue Results	70
5.2 Finite element results	81
5.2.1 Static results	81
5.2.2 Fatigue Results	85
5.2.2.1 Effect of reducing mesh size	86
5.2.2.2 Effect of reducing adhesive thickness	88
CHAPTER SIX	
CONCLUSIONS	90
CONTINUATION STUDIES	92
REFERENCES	92

LIST OF TABLES

Table 2.1: Static experimental testing configurations to assess the influence of the material manufacturing on stainless steel SLJs	13
Table 2.2: Fatigue experimental testing configurations to assess the influence of the surface roughness on stainless steel SLJs	14
Table 2.3: Static experimental testing configurations to assess the influence of the surface roughness on stainless steel SLJs	15
Table 2.4: Fatigue experimental testing configurations to assess the influence of the surface roughness on stainless steel SLJs	15
Table 2.5: Static experimental testing configurations to assess the influence of the material manufacturing on aluminum DLJs	16
Table 2.6: Fatigue experimental testing configurations to assess the influence of the material manufacturing on aluminum DLJs	17
Table 2.7: Single Lap Joints Geometry Data	20
Table 2.8: Double Lap Joints Geometry Data	29
Table 5.1: Effect of material manufacturing on Ultimate Failure Load of Single Lap Joints	56
Table 5.2: Effect of Surface Roughness on Ultimate Failure Load of Single Lap Joints	63
Table 5.3: Effect of material manufacturing on Ultimate Failure Load of Double Lap Joints	68

LIST OF FIGURES

Figure 1.1: Illustration of cleavage and peel loads in adhesively bonded joints	2
Figure 1.2: Additive Manufacturing advantages and disadvantages	5
Figure 1.3: Stress ratio effect on fatigue performance of SLJ	7
Figure 1.4: Algorithm of the numerical method	9
Figure 2.1: Preliminary Design for Substrate Thickness of stainless steel SLJs	19
Figure 2.2: Bending Moment Factor as function of Substrate Thickness for stainless steel SLJs	19
Figure 2.3: Schematic of a Single Lap Joint	20
Figure 2.4: WYKO NT1100 surface profiler	23
Figure 2.5: Calibrated Fixture for Bonding of Adhesive joints	23
Figure 2.6: Preliminary Design for Substrate Thickness of aluminum DLJs	27
Figure 2.7: Bending Moment Factor as function of Substrate Thickness for aluminum DLJs	27
Figure 2.8: Schematic of a Double Lap Joint	28
Figure 2.9: Double Lap Joint placed in the MTS Testing System	31
Figure 3.1: Schematic of C3D8I continuum element	34

LIST OF FIGURES - Continued

Figure 3.2: Spatial representation of a three-dimensional cohesive element	36
Figure 3.3: Contact definition between Adhesive and Adherends	38
Figure 3.4: Lateral view of the DLJ model with load case	38
Figure 3.5: 3D view of the DLJ model	39
Figure 3.6: Traction-separation law shapes	40
Figure 3.7: Schematic damage process zone and corresponding bi-linear traction–separation law	42
Figure 3.8: Different usage of cohesive elements	43
Figure 4.1: Generic SN curve between 10^3 and 10^6 cycles	47
Figure 5.1: Sample Load-Displacement Data for AM-AM Joints	54
Figure 5.2: Sample Load-Displacement Data for WR-WR Joints	54
Figure 5.3: Average Ultimate Load for the two configurations of Single Lap Joints	55
Figure 5.4: Average Shear Stress for the two configurations of Single Lap Joints	55
Figure 5.5: Fatigue performance of Single Lap Joints with AM vs. wrought substrates – Mean load=30% F_u	57

LIST OF FIGURES - Continued

Figure 5.6: Fatigue performance of Single Lap Joints with AM vs. wrought substrates – Mean load=45% Fu	58
Figure 5.7: 3D surface measurement for wrought substrate with higher surface roughness	59
Figure 5.8: 3D surface measurement for wrought substrate with lower surface roughness	60
Figure 5.9: Sample Load-Displacement Data for SLJ made with wrought substrates with higher surface roughness	61
Figure 5.10: Sample Load-Displacement Data for SLJ made with wrought substrates with lower surface roughness	61
Figure 5.11: Average Ultimate Load for the two configurations of Single Lap Joints	62
Figure 5.12: Average Shear Stress for the two configurations of Single Lap Joints	63
Figure 5.13: Effect of Surface Roughness on fatigue performance of Single Lap Joints	64
Figure 5.14: Fracture Surface for Configuration 2 before (left) and after (right) 300000 cycles	65
Figure 5.15: Fracture Surface for Configuration 3 before (left) and after (right) 300000 cycles	66
Figure 5.16: Sample Load-Displacement Data for AM-AM-AM joints	67
Figure 5.17: Sample Load-Displacement Data for AM-EX-AM joints	68

LIST OF FIGURES - Continued

Figure 5.18: Average Ultimate Load for the two configurations of Double Lap Joints	69
Figure 5.19: Average Shear Stress for the two configurations of Double Lap Joints	70
Figure 5.20: Fatigue performance of Double Lap Joints with AM-AM-AM vs. AM-EX-AM substrates – R=0.1	71
Figure 5.21: Fatigue performance of Double Lap Joints with AM-AM-AM vs. AM-EX-AM substrates – R=0.1	72
Figure 5.22: 3D representation of a Double Lap Joint	73
Figure 5.23: SN curves showing the influence of substrate manufacturing on fatigue performance of Double Lap Joints	73
Figure 5.24: Fracture Surface for Configuration 1 (AM-AM-AM)	74
Figure 5.25: Fracture Surface for Configuration 2 (AM-EX-AM)	75
Figure 5.26: 3D surface roughness of an additive manufactured substrate	75
Figure 5.27: Detail of a pore on the additive manufactured surface	76
Figure 5.28: 3D surface measurement of an extruded substrate	77
Figure 5.29: Fracture surface of DLJs cured in autoclave	78
Figure 5.30: Effect of Stress Ratio on fatigue performance of Double Lap Joints	79

LIST OF FIGURES - Continued

Figure 5.31: Effect of Stress Ratio on fatigue performance of Double Lap Joints	80
Figure 5.32: SN curves showing the influence of stress ratio on fatigue performance of Double Lap Joints	80
Figure 5.33: Finite Element Analysis: Double Lap Joint Shear Testing	81
Figure 5.34: Quadratic Nominal Stress Criterion of the Adhesive in the Finite Element Analysis	82
Figure 5.35: Stiffness Degradation of the Adhesive in the Finite Element Analysis	83
Figure 5.36: DLJ placed on the MTS machine with an extensometer	84
Figure 5.37: Comparison Finite Element Analysis vs. Experimental Tests	84
Figure 5.38: Comparison between predicted and experimental values when different maximum loads are applied – AM-AM-AM DLJs (R=0.1)	87
Figure 5.39: Comparison between predicted and experimental values when different maximum loads are applied – AM-EX-AM DLJs (R=0.1)	87
Figure 5.40: Comparison between predicted and experimental values when different maximum loads are applied - AM-EX-AM DLJs (R=0.3)	88
Figure 5.41: Comparison between predicted and experimental values when different maximum loads are applied - AM-AM-AM DLJs (R=0.1)	89
Figure 5.42: Comparison between predicted and experimental values when different maximum loads are applied - AM-EX-AM DLJs (R=0.1)	89

LIST OF FIGURES - Continued

Figure 5.43: Comparison between predicted and experimental values when different maximum loads are applied - AM-EX-AM DLJs (R=0.3) 90

NOMENCLATURE

Latin Symbols

b	Adherend width
b ₁	First fatigue strength exponent
b ₂	Second fatigue strength exponent
E	Young's Modulus
F	Force
G	Shear Modulus
G_{Ic}	Fracture Toughness
k	Bending Moment Factor
L	Overlap Length
l_0	Adherend Length
n	Number of samples
N	Number of fatigue cycles
Nc1	Fatigue transition point
P	Load
R	Stress Ratio
R _a	Average Surface Roughness
S	Stress
SE	Standard Error
SRI1	Stress range intercept
t	Thickness

Greek Symbols

δ	Displacement
σ	Standard deviation

Subscripts

a	Alternating
ad	Adherend
adh	Adhesive
max	Maximum
u	Ultimate

CHAPTER ONE

INTRODUCTION AND LITERATURE SURVEY

1.1 Introduction

For the last few decades, adhesive bonding has been widely used in industrial applications due to their improved mechanical performance. Adhesive bonding can be used in applications as replacement to traditional mechanical fasteners in several sectors, such as aeronautical industry, automotive industry, railway industry, civil industry, marine industry, but also some minor industries like shoes industry. It has many advantages: cost effectiveness, increased design flexibility, ability to join dissimilar materials, continuous contact between surfaces and a more uniform stress distribution. This does not mean that the stresses are constant within the adhesive layer, but that adhesive bonding distributes stresses over the whole bonded region, which leads to lower stress concentrations than in the conventional fastening techniques (bolted, riveted, or welded). At the same time, some disadvantages are associated to adhesive bonding: limited resistance to extreme conditions such as heat and humidity, the need of fixing tools to keep the substrates in position until cure is complete or the fact that frequently adhesive needs high curing temperatures and long curing time. Additionally, to obtain good results, a surface treatment is often required. But the greatest issue is represented by the possibility to have cleavage and peel load, which could lead to poor joint strength.

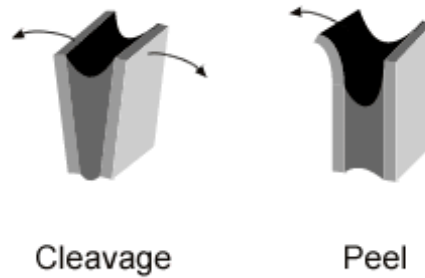


Figure 1.1: Illustration of cleavage and peel loads in adhesively bonded joints

Figure 1.1 shows that cleavage is pull concentrated at one edge of the joint, exerting a prying force on the bond. While one end of the adhesive joint is experiencing concentrated stress on the leading edge, the other edge of the joint is theoretically under zero stress. Cleavage occurs with two rigid substrates. Peel is a pull that is also concentrated at one edge of the joint. One of the substrates is flexible, resulting in even more concentration at the leading edge than with a cleavage joint.

Joints that are well designed for adhesives place a majority of the stress into shear, but also tensile and compression modes are acceptable. This allows the force to be applied over the entire adhesive area. Joints placing stress into cleavage or peel concentrate the stress onto the leading edge. This may lead to premature bond failures, especially if subjected to vibration, impact or fatigue.

Therefore, engineers have different design choices and the most suitable mechanical joint for the specific application must be properly chosen. Additionally, adhesion science involves several technologies and a proper knowledge of many sciences is needed in order to exploit its potential, starting from chemistry and physics and ending with mechanics.

The number of variables involved in order to properly bond the substrates is very wide:

- Surface roughness of the adherends
- Phase change (curing) of the adhesive
- Adhesive's wettability
- Cleaning of the surfaces
- Adhesive type

A large number of theories tries to model what happens locally in the adhesion process. The mechanical and electrostatic interlocking theories state that the surface roughness is one of the parameters which affects the most bonding of the adherends. To select the proper adhesive for a specific application, several factors must be considered. First of all, the function. If the adhesive is a structural adhesive, epoxies, polyurethanes, acrylics are used. Non-structural adhesives, instead, includes rubbers and polyesters. Among the structural adhesives epoxies and polyurethanes are the most spread ones. Epoxies can be one-part or two-part epoxies. They are strong but brittle and they are characterized by low shrinkage. Polyurethanes show a softer behavior, allowing more deformations with respect to epoxies. Wettability is good and also their strength at low temperatures, but they have a limited temperature resistance. The chemical compatibility among the substrates and the adhesive must always be taken into consideration. Then the hardening mechanism and the physical form (liquid, paste, solid) must be considered, together with the method of applications. Cost represents another important variable when choosing the adhesive. In this research, many aspects of the adhesive bonding have been considered: experimental test on real bonded joints have been performed, in order to assess the

influence of material manufacturing and surface roughness on the mechanical performance of the joints. The outputs of some of these tests have been used to build a reliable FE model that allows to characterize the fatigue behavior of the used Non-Commercially Available (NCA) adhesive and to find a methodology in order to predict fatigue life of real patented joints by Stellantis. Part of this study continues the work of a previous study [1], where the same NCA adhesive had been characterized when subjected to static loads.

In particular, in this research, the influence of additive manufacturing on the strength of the joint is studied. Additive manufacturing on 3D printing uses data from CAD software or 3D object scanners to direct hardware to deposit material, layer upon layer, in detailed geometric shapes. As the name implies, additive manufacturing adds material to create an object. On the contrary, when an object is made using traditional means, it is often necessary to remove material.

Additive manufacturing has been around for several decades, since it has great advantages. Really complex parts can be made faster and cheaper with respect to other conventional manufacturing. Additive manufacturing processes are characterized by little lead time: engineers can create a prototype with a 3D printer immediately after finishing the part's stereo lithography (STL) file. As soon as the part has been printed, they may begin testing it instead of waiting several weeks.

Variety is free: if you need to change a part, you can simply modify the original CAD file and the new product can be immediately printed. No assembly is required.

Moving parts can be printed directly into the product, which can significantly reduce the part numbers. Furthermore, because only the material that is needed is used, there is very little material wasted.

But together with the pros additive manufacturing also shows cons. It is characterized by slow build rates. Depending on the part needed, other manufacturing processes may be significantly faster. The production costs are extremely high: sometimes, this is due to the fact that some parts can be made faster using techniques other than additive manufacturing. Therefore, the extra time can lead to higher costs.

Additionally, high-quality additive manufacturing machines can cost hundreds of thousands of dollars together with the material that must be used.

Other issues regard the fact that 3D printed parts often require post-processing: the surface finish and dimensional accuracy may be lower quality with respect to other manufacturing methods. Therefore, it is up to the engineer to decide if additive manufacturing is the right choice for a certain object or if other manufacturing must be considered. In Fig.1.2, a summary of the advantages and disadvantages of using 3D printing.

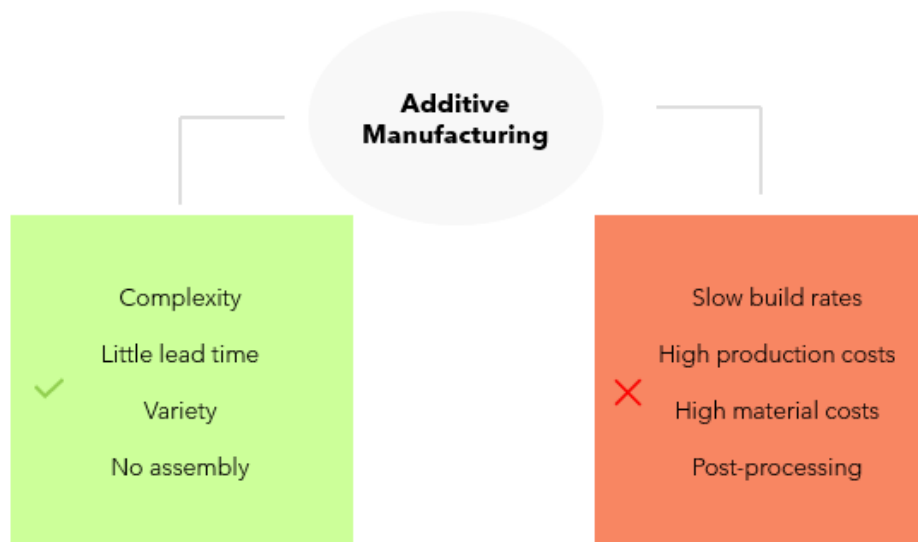


Figure 1.2: Additive Manufacturing advantages and disadvantages

1.2 Literature survey

Many studies have been conducted on adhesive bonded joints: analytical and numerical solutions are used to analyze the stress distribution within the adhesive layer in several configurations of joints, under static and dynamic loads.

Da Silva et al. [2] and [3] summarized the literature about bonding stress evaluation in both Single and Double Lap Joints and addressed the accuracy of strength prediction. The analytical models provided by Volkersen and Goland-Reissner are described [2]. A study case is considered to analyze the stress trend along the overlap length. More complex formulations have been analyzed by the authors in the second paper [3]. The influence of adhesive thickness and overlap length on joint strength is discussed along with experimental testing. Three main study cases are considered: the most interesting one for the sake of this research is the one that considers a SLJ made with high strength steel and a brittle adhesive. For this case of study, the models are able to predict the effect of the overlap length on adhesive strength but they are not able to predict the consequence of increasing the adhesive thickness.

Goglio and Rossetto [4] proposed a solution for Double Lap Joints and compared it with the classical ones found by Volkersen and Hart-Smith. The authors focused on DLJ in order to leave apart aspects related to joint rotation. The goal is to evaluate the approximation on the peak-stresses given by a 1D model, under different combination of overlap length, adhesive thickness and elastic modulus ratio. Finite element results are taken for reference. It is found that their analytical solutions give acceptable results when the elastic modulus of adhesive is much lower than adherends' one.

The behavior of adhesively bonded joints under a dynamic load represents a very interesting and complex topic, therefore many studies focus on the influence that fatigue parameters such as maximum load, mean load, stress ratio or frequency have on the performance of the joints.

Pereira et al. [5] investigated the stress ratio effects on the fatigue behavior of adhesively bonded Single Lap Joints. In this work it was observed that the fatigue life of the adhesive joints has very little dependence on the stress amplitude, indicating that only the maximum stress is important. Indeed, for a fixed fatigue load range, the fatigue life decreases when the mean load (and therefore the maximum) increases. Furthermore, it is observed that the mean shear stress has negligible effect on fatigue strength for a stress ratio $R \leq 0.4$. Afterwards a quadratic formulation seems to be required to fit the experimental results, as shown in Fig.1.3.

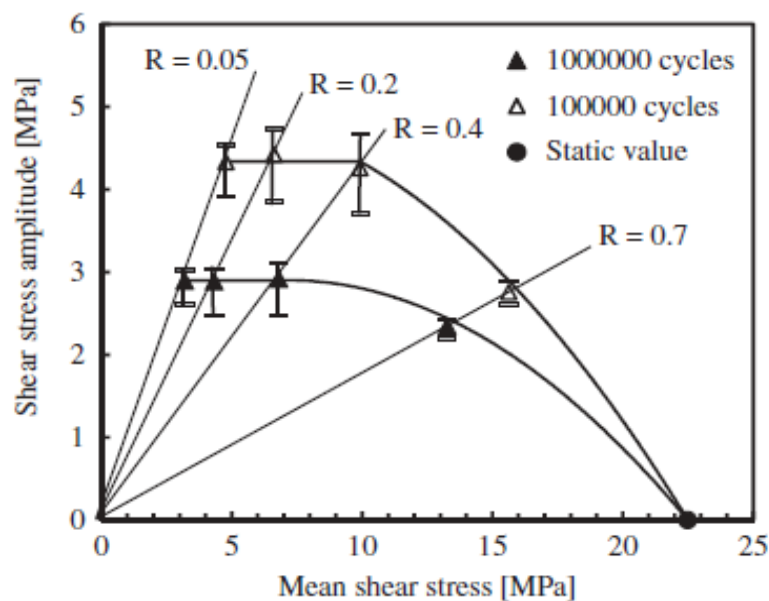


Figure 1.3: Stress ratio effect on fatigue performance of SLJ

Fatigue testing, however, is often costly and time consuming, therefore predictive numerical model can be useful to reduce time and cost. Published literature includes several papers that describe various numerical models. Khoramishad et al. [6] developed a numerical model that accounts for the load ratio effect in constant amplitude fatigue loading, in order to predict the response of these bonded joints. The progressive damage of the adhesive material was modelled using a cohesive zone approach with a bi-linear traction-separation law. Two strain gauges were attached to the substrates at 1mm inside the overlap. These backface strain (non-destructive) gauges provided an independent measure of damage initiation and propagation that was used to validate the models developed. This variable was updated according to a strain-based fatigue damage law for each cycle increment. The initial Young's modulus, the tripping tractions and the fracture energies of the cohesive elements were reduced based on this damage variable. Figure 1.4 shows the algorithm used in this numerical method. Obtained results correlated well with test data on fatigue damage, failure evolution and fatigue life of SLJs.

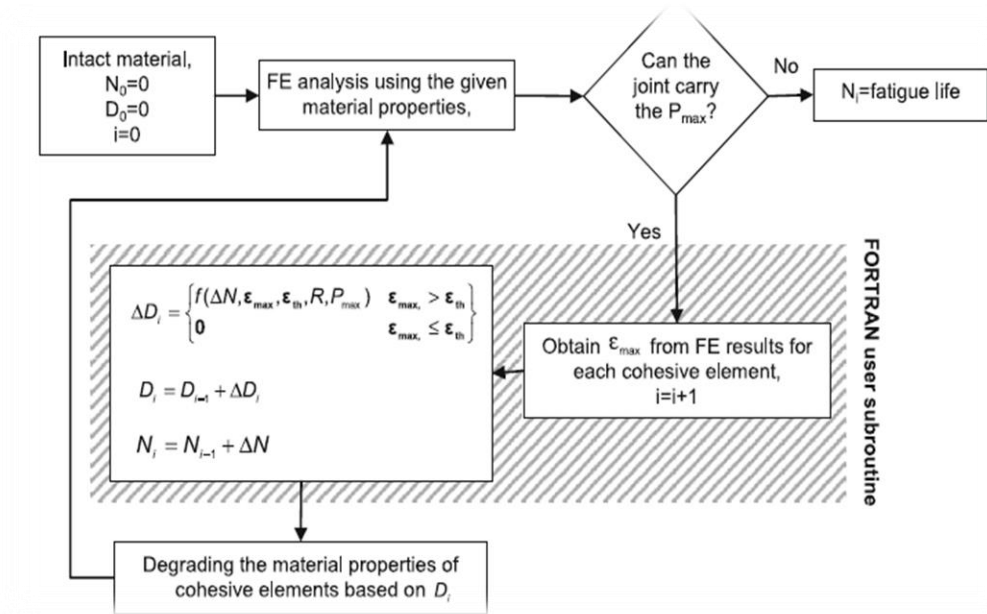


Figure 1.4: Algorithm of the numerical method

De Moura et al. [7] developed a numerical method based on the modified Paris law. Material degradation is simulated with a damage parameter incorporating static and fatigue damage. as a function of loading or time under mixed-mode I+II loading. The numerical crack growth rate was compared with the Paris law used as input under several circumstances, such as different Paris law coefficients and different loading amplitudes. In all cases, it was concluded that the model captures the input Paris law correctly.

1.3 Objectives

The main objective of this research is to analyze and assess, at first glance, how the fatigue performance of different adhesive joints is affected by three main variables: material manufacturing, fatigue parameters and surface roughness. This is done performing several experimental tests.

From these tests, the development of reliable techniques and predictive methodologies for fatigue performance of adhesive joints is performed. Therefore, the main objectives of this study are:

- Perform physical high cycle fatigue tests on Stainless Steel Single Lap Joints and Aluminum Double Lap Joints to investigate and compare different material manufacturing.
- Create an FEA model of DLJs that is able to fit the experimental fatigue test data, providing reliable results.
- Develop a methodology for adhesive joints fatigue life prediction.

Indeed, in the research field, there is a now growing interest in combining adhesive bonding with additive manufacturing. The aim is to achieve an innovative and efficient manufacturing processes, improving the mechanical performance of bonded joints and introducing features to adhesive joints that normally cannot be achieved using traditional manufacturing means.

Research is also being carried out on how to properly bond additively manufactured components, approaching subjects such as surface preparation and geometrical design optimization.

The complexity of the problems of strength prediction of adhesive joints, especially under dynamics loads and in variable environmental conditions, needs to be investigated from several perspectives in order to understand and control the phenomena.

CHAPTER TWO

EXPERIMENTAL SETUP AND TEST PROCEDURE

This work is divided into four main sections. In the first section, the experimental setup and testing procedure is discussed for both the stainless steel SLJs and the aluminum DLJs. The second section outlines the finite element modeling of DLJs using Abaqus Software package. Methodology and software for fatigue life prediction is outlined in the third section. In the section four, experimental data is generated and plugged into the virtual models proposed to assess parameter influence on fatigue life; main parameters include substrate manufacturing and surface roughness. Therefore, this chapter will focus on the experimental setup and test procedure adopted for adhesively bonded single lap joints and double lap joints.

Lap shear tests and constant amplitude fatigue tests have been performed on different configurations of joints, since one of the main goals of this study is to assess the influence of the material manufacturing on fatigue performance. Also, an additional experimental plan involving single lap joints has been designed, in order to investigate the influence of the surface roughness on static and fatigue performance.

2.1 Experimental procedure

This research can be divided in two main parts. In the first part, Single Lap Joints made with additive manufactured 17-4 PH stainless steel and SLJs made with wrought 17-4 PH stainless steel have been manufactured. The purpose of the experiments for the SLJs is to evaluate the influence of the material manufacturing and surface roughness on the fatigue strength of the joints, while the other key design

variables, such as adhesive thickness and overlap length, remain constant. The considered adhesive is the commercially available Betamate 73326M, a two-component epoxy-based adhesive.

In order to assess how the surface roughness influences the performance of the joints, an additional experimental plan involving the single lap joints made with wrought 17-4 PH stainless steel has been designed. To fulfill this goal, two configurations of joints have been considered. In the first configuration, the single lap joints are made with wrought 17-4 PH stainless steel substrates and the value of the average surface roughness R_a is roughly 500 nm. In the second configuration, the single lap joints are made with wrought 17-4 PH stainless steel substrates, but the value of the average surface roughness R_a is between 50 nm and 100 nm. Indeed, the purpose of the experiments for the SLJs is to assess the influence of the surface roughness on the static and fatigue strength of the joints, while the other key design variables, such as adhesive thickness and overlap length, remain constant. Therefore, the main outputs of the static and fatigue testing for the SLJs will be the respectively the average shear strength and SN curve obtained for each considered configuration.

An experimental plan involving double lap joints has been designed for the second part of this research, in order to properly parametrize the epoxy-based adhesive used in this study. The purpose of DLJ testing is to assess the influence of the material manufacturing on fatigue life; the other key design variables, such as adhesive thickness and overlap length, remain constant. The results obtained with additive manufacturing aluminum substrates are compared with that obtained testing a mixed configuration, where an extruded middle substrate is bonded to the two 3D

printed substrates. SN curves and data are used for the development of a methodology for fatigue life prediction using finite element modelling.

Table 2.1: Static experimental testing configurations to assess the influence of the material manufacturing on stainless steel SLJs

<i>Joint configurations</i>			<i>Adhesive bonding</i>		
Sample size	Material	Adherend thickness [mm]	Adhesive thickness [mm]	Overlap length [mm]	Adhesive type
2	AM-AM	1.587	0.2	25.4	Two-component epoxy
4	WR-WR	1.587	0.2	25.4	Two-component epoxy

Table 2.2: Fatigue experimental testing configurations to assess the influence of the surface roughness on stainless steel SLJs

<i>Joint configurations</i>			<i>Fatigue parameters</i>		
Sample size	Material	Adhesive type	Alternating Load [% F _u]	Mean Load [% F _u]	Frequency [Hz]
3	AM-AM	Two-component epoxy	20%	45%	10
3	AM-AM	Two-component epoxy	15%	45%	10
3	AM-AM	Two-component epoxy	10%	45%	10
3	WR-WR	Two-component epoxy	25%	30%	10
3	WR-WR	Two-component epoxy	20%	30%	10
3	WR-WR	Two-component epoxy	15%	30%	10

Table 2.3: Static experimental testing configurations to assess the influence of the surface roughness on stainless steel SLJs

<i>Joint configurations</i>			<i>Adhesive bonding</i>		
Sample size	Material	Average surface roughness R_a [nm]	Adhesive thickness [mm]	Overlap length [mm]	Adhesive type
4	WR-WR	500	0.2	25.4	Two-component epoxy
4	WR-WR	50÷100	0.2	25.4	Two-component epoxy

Table 2.4: Fatigue experimental testing configurations to assess the influence of the surface roughness on stainless steel SLJs

<i>Joint configurations</i>			<i>Fatigue parameters</i>		
Sample size	Material	Average surface roughness R_a [nm]	Alternating Load [% F_u]	Mean Load [% F_u]	Frequency [Hz]
3	WR-WR	500	20%	45%	10
3	WR-WR	500	15%	45%	10
3	WR-WR	500	10%	45%	10
3	WR-WR	50÷100	20%	45%	10
3	WR-WR	50÷100	15%	45%	10

Table 2.4 - Continued

<i>Joint configurations</i>			<i>Fatigue parameters</i>		
Sample size	Material	Average surface roughness Ra [nm]	Alternating Load [% Fu]	Mean Load [% Fu]	Frequency [Hz]
3	WR-WR	50÷100	10%	45%	10

Table 2.5: Static experimental testing configurations to assess the influence of the material manufacturing on aluminum DLJs

<i>Joint configurations</i>			<i>Adhesive bonding</i>		
Sample size	Material	Adherend thickness [mm]	Adhesive thickness [mm]	Overlap length [mm]	Adhesive type
4	AM-AM-AM	6	0.5	12.7	NCA Single Part epoxy
4	AM-EX-AM	6	0.5	12.7	NCA Single Part epoxy

Table 2.6: Fatigue experimental testing configurations to assess the influence of the material manufacturing on aluminum DLJs

<i>Joint configurations</i>			<i>Fatigue parameters</i>		
Sample size	Material	Adhesive type	Maximum Load [% F _u]	Stress Ratio	Frequency [Hz]
4	AM-AM-AM	NCA Single Part epoxy	70%	0.1	10
4	AM-AM-AM	NCA Single Part epoxy	60%	0.1	10
4	AM-AM-AM	NCA Single Part epoxy	50%	0.1	10
4	AM-EX-AM	NCA Single Part epoxy	70%	0.1	10
4	AM-EX-AM	NCA Single Part epoxy	60%	0.1	10
4	AM-EX-AM	NCA Single Part epoxy	50%	0.1	10
3	AM-EX-AM	NCA Single Part epoxy	75%	0.3	10
3	AM-EX-AM	NCA Single Part epoxy	65%	0.3	10
3	AM-EX-AM	NCA Single Part epoxy	55%	0.3	10

2.2 Single Lap Joint Test

2.2.1 Joint Geometry

Test Single Lap Joint configurations are described in this section.

The first design choice is about the geometry of the specimens that varies according to the characteristics of the adhesive. The values of the adhesive thickness, joint width and overlap lengths are standardized, while the adherend thickness must be carefully selected. Indeed, to investigate the behavior of the adhesive, the adherend thickness must be such that the adherend yield load is larger than the adhesive one. In order to evaluate the correct adherend thickness, Adams' failure criterion [8] has been exploited and different bending moment factors formulations have been implemented in the model. All the equations coming from the Adams criterion [8] have been implemented in MATLAB. The design tool assessed that the minimum value of the adherend thickness for the tests that allows to avoid yielding in the substrates is 0.55 mm: for lower adherend thickness, the yielding load would be reached first in the adherends with respect to the adhesive. Therefore, it has been decided to use substrates with an adherend thickness equal to 1.587 mm (1/16"), that is above the minimum limit value. In Fig.2.1, the value of the substrate thickness after the interception is the minimum value that guarantees the yielding of the adhesive to occur first with respect to the yielding of the substrates. In Fig.2.2 the different bending moment factors implemented in the study are represented. The most conservative formulation (Goland-Reissner) has been chosen among all the factors.

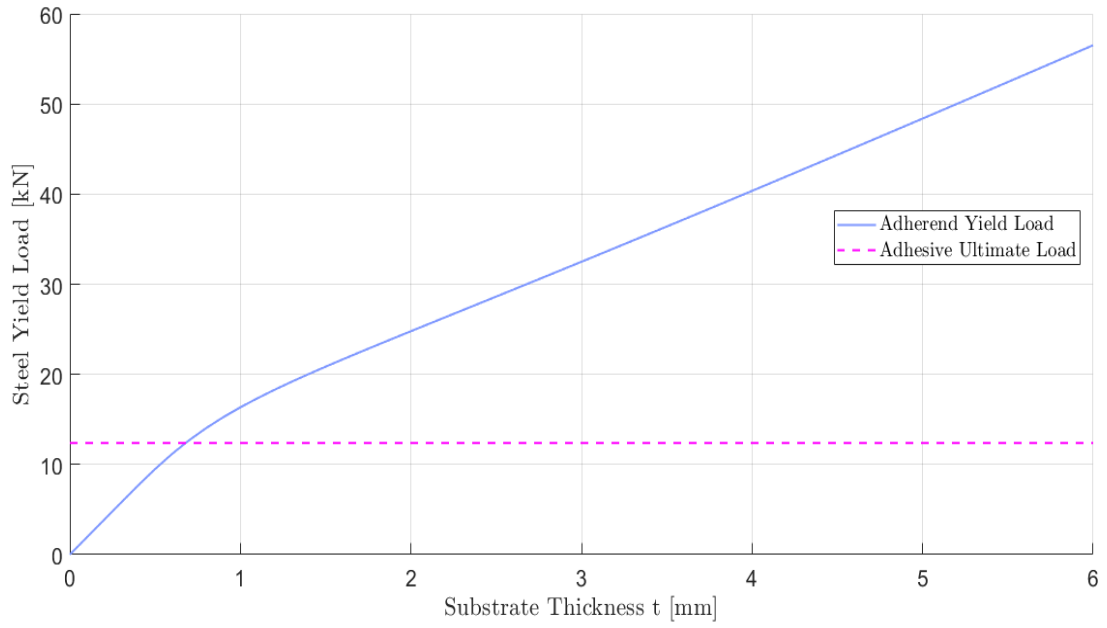


Figure 2.1: Preliminary Design for Substrate Thickness of stainless steel SLJs

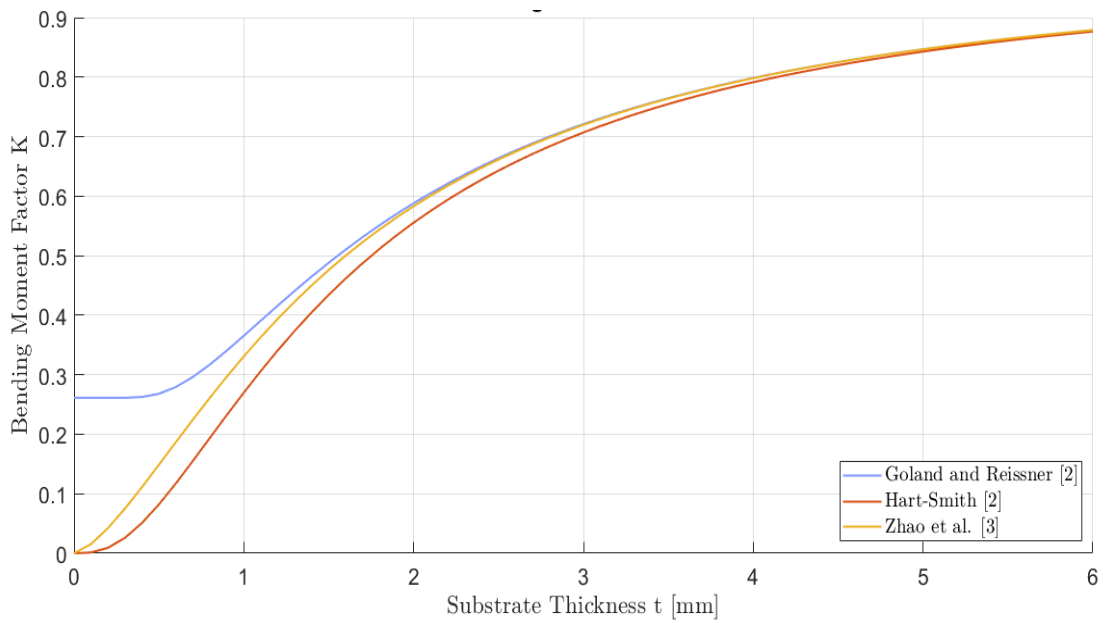


Figure 2.2: Bending Moment Factor as function of Substrate Thickness for stainless steel SLJs

Figure 2.3 shows a schematic representation of the Single Lap Joint, that is the same for both the configurations. All the geometry data are reported in Table 2.7.

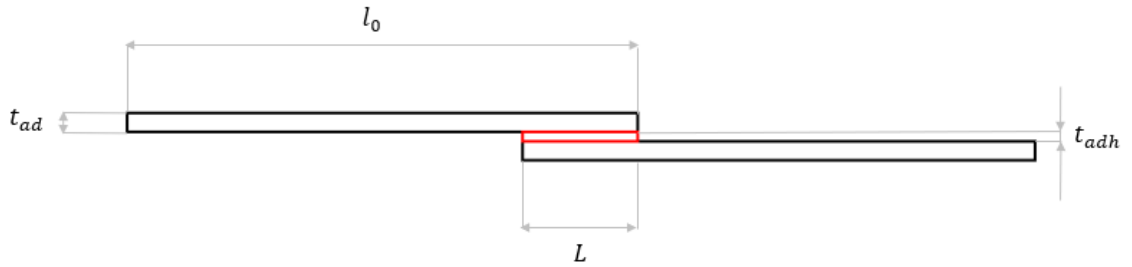


Figure 2.3: Schematic of a Single Lap Joint

Table 2.7: Single Lap Joints Geometry Data

Adherend Width b [mm]	25.4
Overlap Length L [mm]	25.4
Adherend Length l_0 [mm]	101.6
Adherend Thickness t_{ad} [mm]	1.587
Adherend Young Modulus E [MPa]	210000
Adhesive Thickness t_{adh} [mm]	0.2

2.2.2 Bonding Process

The proper adhesion of the substrates' surfaces is a complicated process, essential to achieve reliable results. The adherends' preparation is a fundamental step that could affect significantly the performance and the failure mode of the joint from adhesive to cohesive. Usually, the surface roughness of the adherends is unified using sand paper or an electric wire brush.

In this study, for the Configuration 1 of SLJs the additive manufactured adherends have been prepared using an electric wire brush, in order to remove the oxide layers present on the surface of the steel substrates. After this, the substrates have been carefully cleaned with acetone to remove any grease stain present on the surface. The average surface roughness of these SLJs has been measured using the WYKO NT1100 optical profiler system, shown in Fig.2.4 below. Its value is roughly equal to 3.5 μm .

For the SLJs of Configuration 2, the same process has been repeated: both the additive manufactured and the wrought adherends have been prepared using an electric wire brush. Also in this case, the substrates have been carefully cleaned with acetone before proceeding with the bonding process. For this configuration, the average surface roughness measured using the WYKO NT1100 optical profiler system, is roughly equal to 500 nm.

In order to investigate the influence of the surface roughness on the static and fatigue performance of the joints, the wrought adherends have been prepared following a different procedure. For the Configuration 3, initially, an electric wire brush has been used. Then, firstly a very coarse sand paper and then a very fine sand paper (1000 grit) have been accurately rubbed on the substrates, in order to reduce significantly the

value of the average surface roughness. This has been carefully measured for all the substrates using the WYKO NT1100 optical profiler system, in order to be sure that the value was between 50 nm and 100 nm.

As in the previous case, the substrates have been carefully cleaned with acetone before proceeding with the bonding process.

The bonding of the substrates has been realized exploiting a calibrated fixture that is able to guarantee the overlap length (25.4 mm) and the correct alignment of the substrates. Figure 2.5 shows a 3D view of the calibrated fixture. Calibrated aluminum spacers have been used to guarantee the required thickness room for the adhesive (0.2 mm). The adhesive used for this research is a two-component epoxy adhesive. The curing has been performed in oven, at 60°C for 120 minutes. Calibrated weights have been placed on the bonding area to guarantee proper pressure on the bonding surfaces.



Figure 2.4: WYKO NT1100 surface profiler

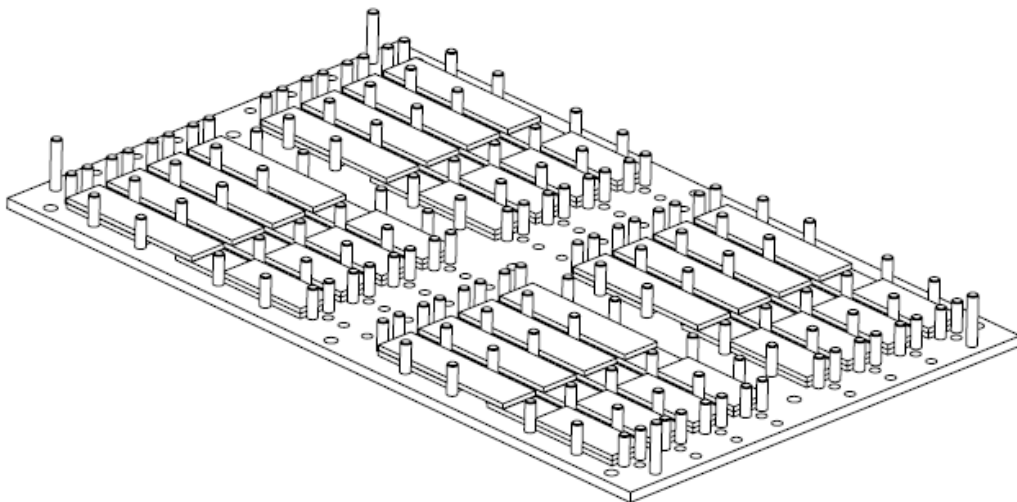


Figure 2.5: Calibrated Fixture for Bonding of Adhesive joints

2.2.3 Quasi-static Shear-Tensile Tests

In this section, the procedure and the parameters used to perform Quasi-Static Shear-Tensile Tests on the SLJs are described. Once the SLJ specimen has been prepared, calibrated tabs are used to align the specimen in the testing machine. The Shear-Tensile Tests have been conducted using an MTS machine, with a strain rate of 1.27 mm/min to reproduce a quasi-static test. Figure 2.6 shows a SLJ placed in the MTS machine.

For what concerns the SLJ geometry, as reported in Table 2.7, the substrates are 25.4 mm (1") wide and 101.6 mm (4") long, the overlap between the substrates is equal to 25.4 mm (1"). The adhesive thickness is equal to 0.2 mm. These values are fixed for all the configurations and remain constant for all the tests. For each configuration, 4 quasi-static Shear-Tensile Tests have been performed.

2.2.4 Fatigue Testing

In this section, the procedure and the parameters used to perform high cycle fatigue tests on the SLJs are described. Fatigue Shear-Tensile Tests have been conducted using the same MTS machine. As reported in Table 2.2, for the same value of mean load, three levels of maximum load have been investigated, in order to compare the performance of Configuration 1 and Configuration 2 of Single Lap Joints. The two values of mean load are equal to 45% and 30% of the average ultimate load. When the mean load is equal to 45%, the alternating loads are equal to 20%, 15%, 10% of the average ultimate load of each configuration. Instead, when the mean load is equal to 30%, the alternating loads are set equal to 25%, 20%, 15% of the average ultimate load of each configuration. In order to obtain a more reliable SN curve for each configuration, three repetitions have been performed for each point.

Then, for Configuration 3, only the fatigue tests with mean load equal to 45% have been performed. The main goal is to study and assess the influence of surface roughness on the static and fatigue behavior of the joints, comparing the results with the ones obtained for Configuration 2, when the same mean and alternating loads are applied on the two configurations. The frequency is set to 10 Hz.



Figure 2.6: MTS Fatigue Testing System for SLJs

2.3 Double Lap Joint Test

2.3.1 Joint Geometry

In this section, the geometry of the Double Lap Joints is described.

The geometry of the specimens varies according to the characteristics of the adhesive. The values of the adhesive thickness, joint width and overlap lengths are standardized, while it is necessary to repeat the calculations and evaluate the adherend thickness, since both the adherends and the adhesive used for these joints have mechanical properties different from the ones used to bond the SLJs. Indeed, since one of the aims of this part of the research is to characterize the Non-Commercially Available adhesive, the adherend thickness must be such that the adherend yield load is larger than the adhesive one.

Adams' failure criterion [8] is implemented in MATLAB, for obtaining the minimum value of the adherend thickness of test samples in order to avoid yielding of substrate material during fatigue tests. The design tool assessed that the minimum value of the adherend thickness for the tests that allows to avoid yielding in the substrates is 6 mm: for lower adherend thickness, the yielding load would be reached first in the adherends with respect to the adhesive. Therefore, this led to using an adherend thickness equal to 6 mm.

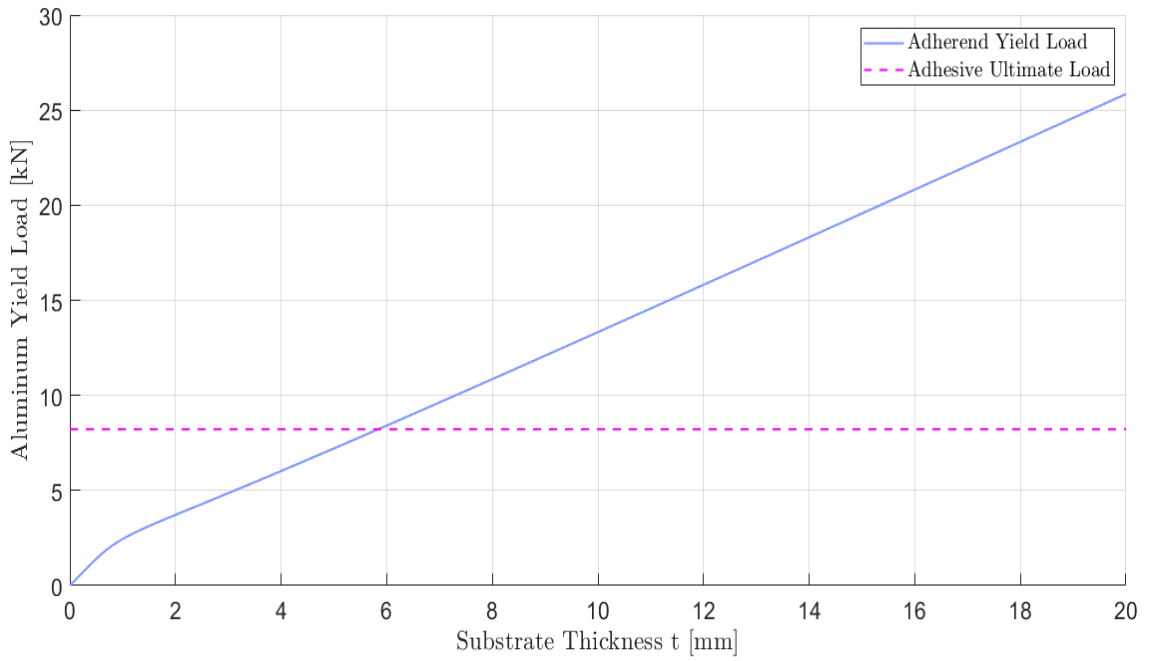


Figure 2.6: Preliminary Design for Substrate Thickness of aluminum DLJs

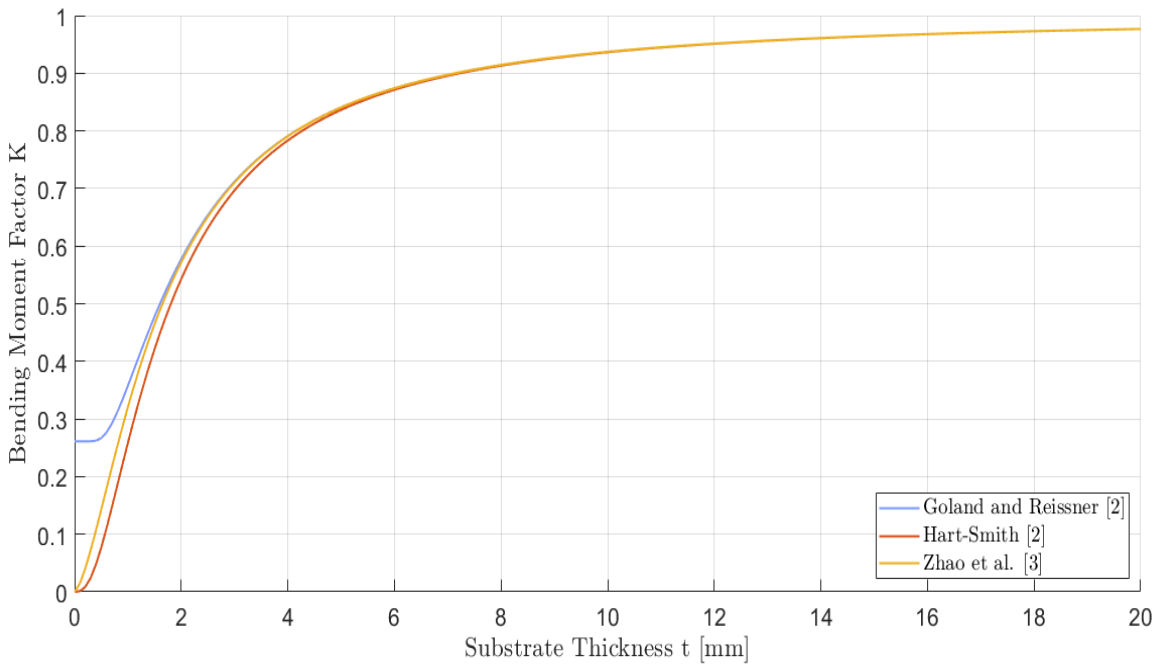


Figure 2.7: Bending Moment Factor as function of Substrate Thickness for aluminum DLJs

As in the case of Single Lap Joints, in Fig.2.6, the value of the substrate thickness after the interception is the minimum value that guarantees the yielding of the adhesive to occur first with respect to the yielding of the substrates. In Fig.2.7 the different bending moment factors implemented in the study are represented. From the graph, it is clear that all the factors converge to the same value as the joint thickness increases. On the contrary, for low thicknesses a significant difference is noticeable among the different bending moment factors. In this study [1], the most conservative formulation (Goland-Reissner) has been chosen among all the factors.

Figure 2.8 shows a schematic representation of the Double Lap Joint, that is the same for both the configurations. Table 2.8 reports all the geometry data.

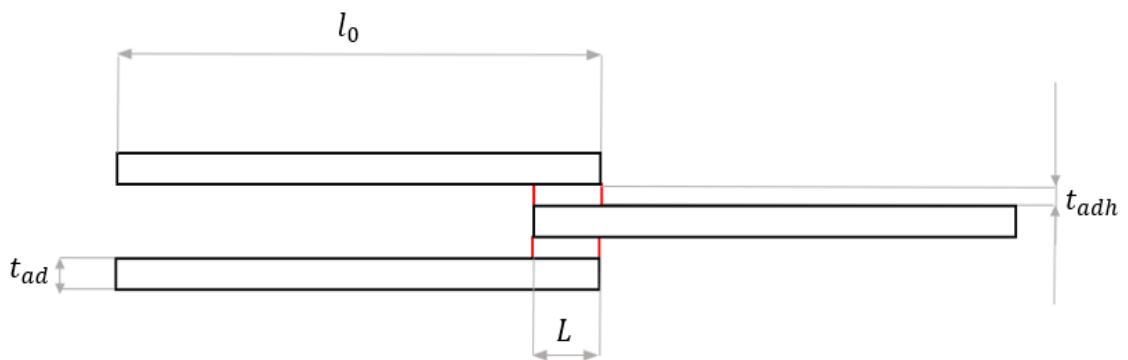


Figure 2.8: Schematic of a Double Lap Joint

Table 2.8: Double Lap Joints Geometry Data

Adherend Width b [mm]	25.4
Overlap Length L [mm]	12.7
Adherend Length l_0 [mm]	101.6
Adherend Thickness t_{ad} [mm]	6
Adherend Young Modulus E [MPa]	70000
Adhesive Thickness t_{adh} [mm]	0.5

2.3.2 Bonding Process

For Configuration 1 (AM-AM-AM) of DLJs the adherends have been prepared using an electric wire brush, in order to remove the oxide layers present on the surface of the Additive Manufactured aluminum substrates. After this, the substrates have been carefully cleaned with acetone to remove any grease stain present on the surface. For the DLJs of Configuration 2, the exact same process has been repeated. Both the additive manufactured and the extruded adherends have been prepared using an electric wire brush. Also in this case, the substrates have been carefully cleaned with acetone before proceeding with the bonding process.

The bonding of the substrates has been realized exploiting a calibrated fixture that is able to guarantee the overlap length (12.7 mm) and the correct alignment of the substrates. Calibrated aluminum spacers have been used to guarantee the required thickness room for the adhesive (0.5 mm). The adhesive used for this research is a NCA One Part epoxy adhesive. The curing has been performed in oven, at 180°C for 30 minutes. Calibrated weights have been placed on the bonding area to guarantee proper pressure on the bonding surfaces.

2.3.3 Quasi-static Shear-Tensile Tests

In this section, the procedure and the parameters used to perform Quasi-Static Shear-Tensile Tests on the DLJs are described. Once the DLJ specimen has been prepared, calibrated tabs are used to align the specimen in the testing machine. The Shear-Tensile Tests have been conducted using an MTS machine, with a strain rate of 1.27 mm/min to reproduce a quasi-static test. Figure 2.9 shows a DLJ placed in the MTS machine.

For what concerns the DLJ geometry, as reported in Table 2.3, the substrates are 25.4 mm (1") wide and 101.6 mm (4") long, the overlap between the substrates is equal to 12.7 mm (1/2"). The adhesive thickness is equal to 0.5 mm. These values are fixed for both the configurations and remain constant for all the tests. For each configuration, 4 quasi-static Shear-Tensile Tests have been performed.

2.3.4 Fatigue Testing

In this section, the procedure and the parameters used to perform high cycle fatigue tests on the DLJs are described. The fatigue Shear-Tensile Tests have been conducted using the same MTS machine. As reported in Table 2.6, for the same value of stress ratio, three levels of maximum load have been investigated, in order to compare the performance of the two configurations of Double Lap Joints. The stress ratio R is equal to 0.1. The maximum loads are equal to 70%, 60%, 50% of the average ultimate load of each configuration. In order to obtain a more reliable SN curve for each configuration, 4 repetitions have been performed for each point. Then, only for the Configuration 2 (mixed configuration) of Double Lap Joints, fatigue tests with a different value of stress ratio have been performed, in order to assess its influence on the fatigue performance of the joints. In this case, three levels of

maximum load have been investigated: these are equal to 75%, 65%, 55% of the average ultimate load of the mixed configuration. The value of the stress ratio R is equal to 0.3. The frequency is set to 10 Hz.



Figure 2.9: Double Lap Joint placed in the MTS Testing System

CHAPTER THREE

FINITE ELEMENT MODELS

This chapter will focus on the procedure and workflow used to realize the finite element models of the adhesively bonded joint. Two FEA models are used; the first model uses cohesive zone elements are used for the adhesive. Linear elastic elements are used in the second model for Design Life analysis using nCode software, which does not recognize cohesive zone elements.

3.1 Finite Element Modeling

In order to predict the strength and the mechanical behavior of an adhesively bonded joint, the stress distribution and a suitable failure criterion are needed. The stress distribution can be obtained by a closed-form model or finite element analysis. The mechanical behavior of adhesively bonded joints is not only influenced by the geometry of the joints but also by different boundary conditions. The increasing complex joint geometry and its three-dimensional nature increase the difficulty of obtaining an overall system of governing equations for predicting the strength and the mechanical properties of the adhesively bonded joints. In addition, material non-linearity due to plastic behavior leads to a very complex analysis. Therefore, for a fast and easy answer, a closed-form analysis is more suitable, but for complex geometries and elaborate material models, a numerical model like FEA is preferable.

The greatest advantage of the FEA is that the mechanical properties in an adhesively bonded joint of almost any geometrical shape under various load conditions can be determined. For what concerns accuracy of the results, this has a great dependence on the mesh size of the FEA model. Typically, the smaller the mesh size, the more

accurate the solution. The trade-off is that the higher the accuracy, the larger become the simulation and thus computational time is extended.

In the case of adhesively bonded joints, generally the thickness of adhesive layer is much smaller than the one of the adherends. It is essential to model the adhesive layer by a finite element mesh which is smaller than the mesh size used for the rest of the joint. As a result, in a very small region the finite element mesh can be orders of magnitude more refined than is needed in the rest of the joint. In this case, it is also important that a smooth transition between the adherends and adhesive is provided. Therefore, studies are needed to obtain the optimal balance between accuracy and computational cost.

In this research, in order to properly catch the physics of the problem and, at the same time, to have a mesh size that can be used for a real component that must be inserted in a full-vehicle model, for the adherends of the Double Lap Joints, 2mm elements have been used. Instead, the mesh of the adhesive was built with 1mm elements.

3.2 Double Lap Joints

The workflow to build the finite element model for the Double Lap Joint requires the following steps to be performed:

- CAD Geometry Definition
- Geometry Import and Clean Up
- Mesh Creation
- Set Segments and Groups Creation (Contact Surfaces) among Adhesive and Adherends
- Materials and Properties Definition
- Load Case Definition and Simulation Run

SOLIDWORKS is used to realize the DLJ geometry. The geometry is subsequently imported in HYPERMESH. The software used to run the simulation is ABAQUS.

The realized model exploits a 3D mesh. The elements used to represent the mechanical behavior of the adherends are C3D8I, full integration hexagonal elements.

Five aspects of an element characterize its behavior:

- Family
- Degrees of freedom (directly related to the element family)
- Number of nodes
- Formulation
- Integration

Each element in Abaqus has a unique name, which identifies each of the five aspects of an element.

C3D8I is a Continuum element; first letter of the element designation refers to the element family. Figure 3.1 shows a schematic of a continuum element, used for the DLJ models.

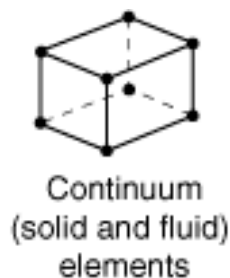


Figure 3.1: Schematic of C3D8I continuum element

The degrees of freedom are the fundamental variables calculated during the analysis.

Displacements or other degrees of freedom are calculated at the nodes of the element.

At any other point in the element, the displacements are obtained by interpolating

from the nodal displacements. Usually, the interpolation order is determined by the number of nodes in the element. Elements that have nodes only at their corners, such as the 8-node brick elements C3D8I, use linear interpolation in each direction and are often called linear elements or first-order elements.

An element's formulation refers to the mathematical theory used to define the element's behavior. In the Lagrangian, or material, description of behavior the element deforms with the material. Instead, in the alternative Eulerian, or spatial, description elements are fixed in space as the material flows through them. These latter methods are commonly used in fluid mechanics simulations.

Concerning the integration, Abaqus uses numerical techniques to integrate different quantities over the volume of each element, allowing in this way a complete overview in material behavior. Abaqus evaluates the material response at each integration point in each element. Some continuum elements in Abaqus can use full or reduced integration. This can have a significant effect on the accuracy of the element for a given problem. C3D8I elements use full integration and guarantee more precision on the calculus, even if at the expense of higher computational cost.

As already mentioned, instead, for the adhesive, two types of elements have been chosen. In the first model, 8-node three-dimensional cohesive elements COH3D8 are used to simulate the adhesion bond between the adhesive and adherends. Figure 3.2 shows the spatial representation of a three-dimensional cohesive element:

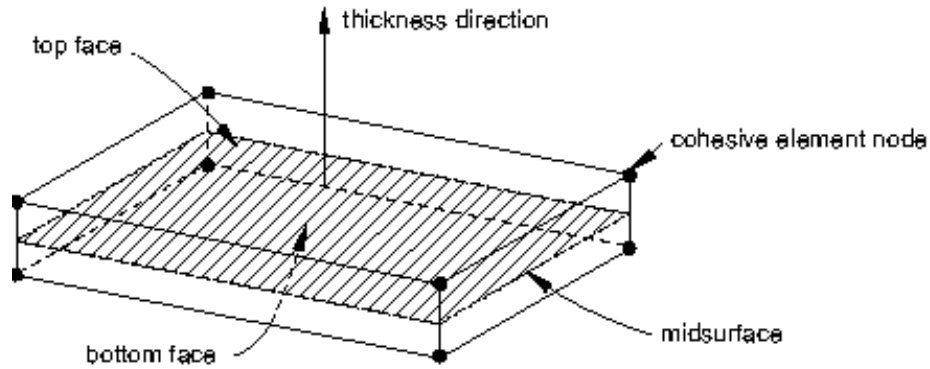


Figure 3.2: Spatial representation of a three-dimensional cohesive element

The connectivity of cohesive elements is the same of continuum elements, but it is useful to think of cohesive elements as being composed of two faces separated by a thickness. The relative motion of the bottom and top faces measured along the thickness direction represents opening or closing of the interface. The relative change in position of the bottom and top faces measured in the plane orthogonal to the thickness direction quantifies the transverse shear behavior of the cohesive element. In the second model, linear elastic C3D8I elements have been used for the adhesive too.

So far, the first model considered 2 mm elements for the adherends and 1 mm cohesive elements for the adhesive. The second model considered 2 mm elements for the adherends and different mesh sizes for the adhesive. Indeed, a sensitivity analysis has been carried on in order to investigate the effect of the increased discretization on the results. After the clean-up and meshing of the DLJ geometry, it is possible to define the surfaces which are going to simulate the contact interaction between adhesive and adherends. Indeed, the fundamental part of the modeling is the contact definition (TIE) among the two adhesive-adherend interfaces of the DLJ.

A TIE constraint ties two separate surfaces together so that there is no relative motion between them. Indeed, a surface-based TIE constraint can be used to make the translational and rotational motion as well as all other active degrees of freedom equal for a pair of surfaces. By default, nodes are tied only where the surfaces are close to one another. One surface in the constraint is designated to be the slave surface, while the other surface is the master surface. This type of constraint allows to fuse together two regions even though the meshes created on the surfaces of the regions may be dissimilar. It is possible to define a TIE contact between edges of a wire or between faces of a solid or shell.

In this study, TIE constraint has been chosen since it can perfectly simulate two surfaces that are bonded together. Therefore, set segments (Contact Surfaces) have been created and collected in groups (TIE), assigning the slave surface to the part yielding at lower stress (i.e. the adhesive) and the master surface to the adherends. In Fig.3.3 the contact definition among the two adhesive-adherend interfaces of the DLJ is shown. The connection among the adhesive and adherends could have been realized also by simply aligning the nodes of the elements and making them coincident, but creating the groups allows to have more freedom on the meshing of the surfaces. After the set segments and groups creation, the adherend material properties are defined. The Young modulus E and several points of the curve $\sigma - \varepsilon$ are given as input to characterize respectively the elastic and the plastic behavior of the considered additive manufactured AlSi10Mg aluminum. Instead, concerning the adhesive, when Cohesive Zone Elements are used, several parameters are used as input to combine the effect of the fracture mechanics and material strength approach. This theme will be deepened in the following section.

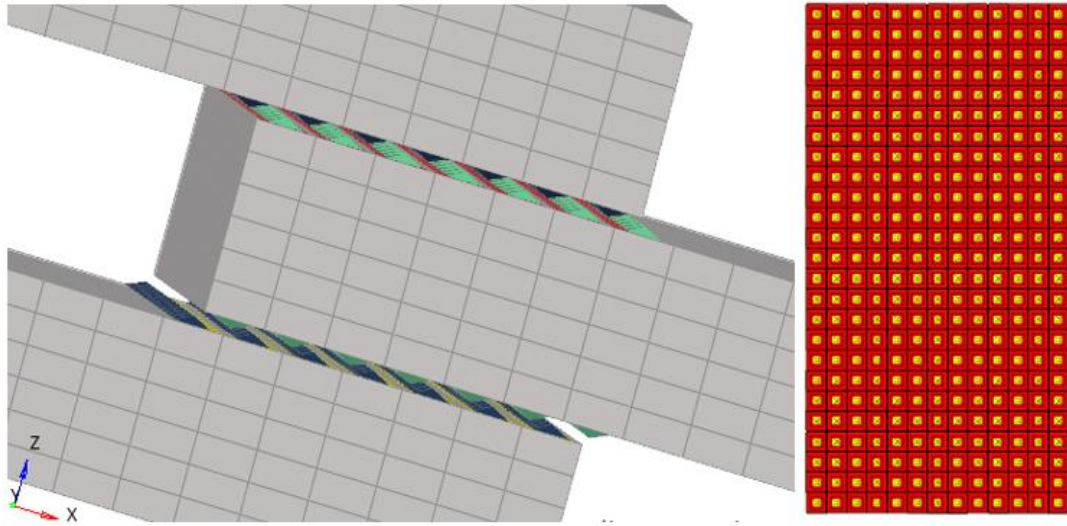


Figure 3.3: Contact definition between Adhesive and Adherends

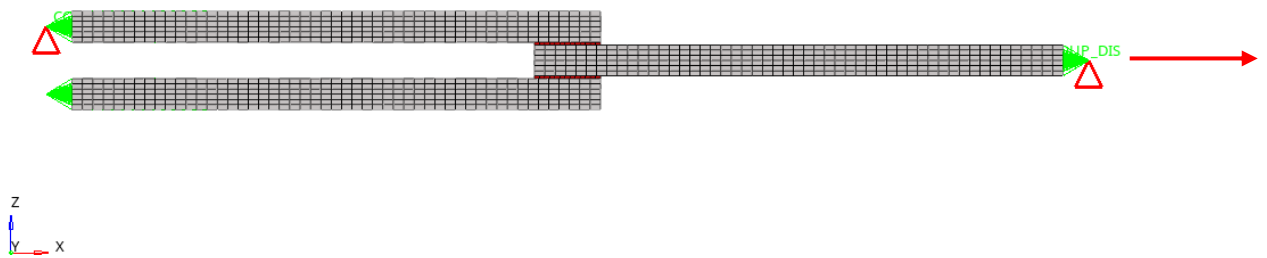


Figure 3.4: Lateral view of the DLJ model with load case

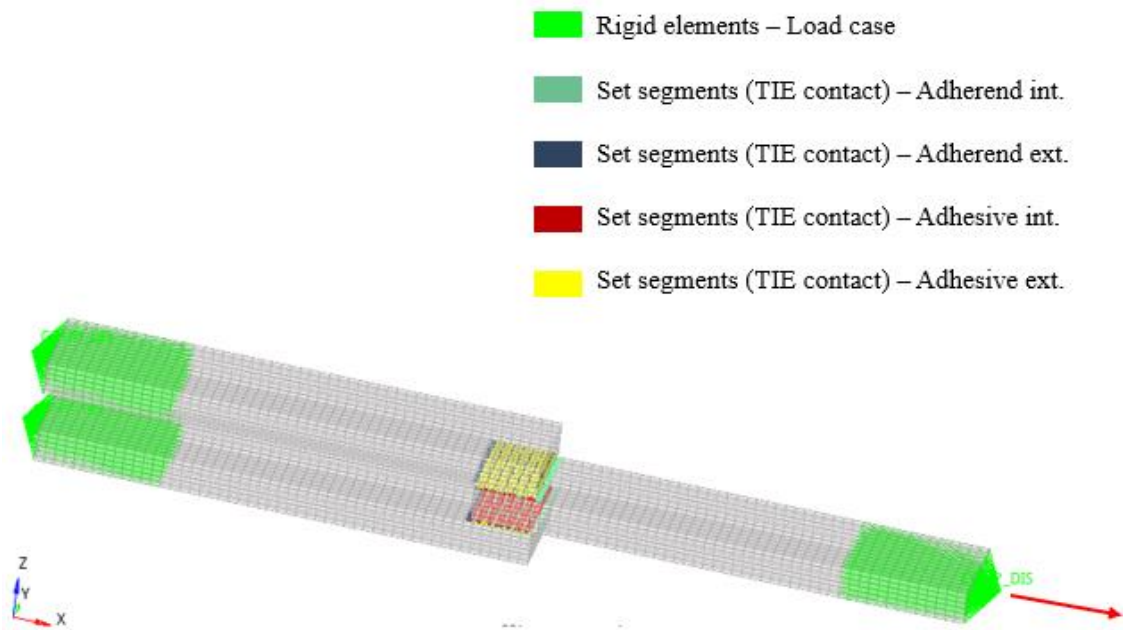


Figure 3.5: 3D view of the DLJ model

As Figures 3.4 and 3.5 show, the load case applied to the Double Lap Joint simulates the lap shear stress test, constraining all the nodes in the grip (6 dofs) with 1D rigid elements (RBE3) from one side (left side) and displacing from the other side (right side) until the failure of the joint is verified.

Once defined the material properties and the load case, it is possible to run the simulation using as solver ABAQUS.

3.2.1 Cohesive Zone Modeling

Cohesive Zone Modeling (CZM) is a powerful tool that has recently received considerable attention. It can be employed for a wide variety of problems, such as predicting delamination in adhesively bonded structures; it can be used with several materials including metals, ceramics, polymers and composites. The Cohesive Zone Model was developed in a continuum damage mechanics context and used fracture

mechanics concepts to improve its applicability. In a CZM approach, fracture is assumed to occur by progressive separation of the crack surfaces ahead of the crack tip. The Crack propagation occurs when the crack separation reaches a critical value δ_c . Several Cohesive Zone Models have been developed in the last years. The key input into any Cohesive Zone Model is the traction-separation law (TSL). Indeed, the successful use of Cohesive Zone Modeling relies upon the shape of the traction-separation law, which must be able to represent accurately the fracture of the material or interface being modeled, allowing an accurate strength prediction. The shapes of traction-separation proposed in the different models include bi-linear (triangular), trapezoidal, linear-exponential, exponential and polynomial forms. Some of these are shown in Fig.3.6.

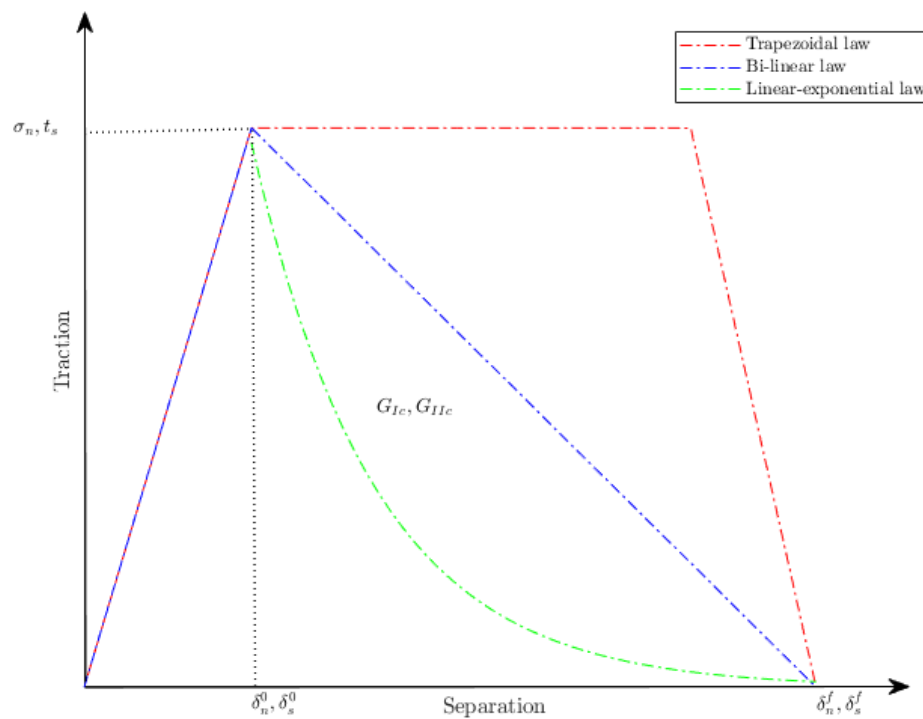


Figure 3.6: Traction-separation law shapes

The choice of the traction-separation law depends on the case of study and its parameters can be adjusted depending on the behavior of the material or interface to get more precise results. Using more complex laws can result in more convergence problems and more time to carefully calibrate the larger number of parameters to be set, but with more precise results. Therefore, depending on the case of study, a trade-off is necessary. However, some researchers [9,10] concluded that the influence of the shape can be disregarded, but other researchers [11,12] highlighted that shape of the strain-softening branch can significantly influence the results.

In this study, the adhesive showed a quasi-brittle behavior. Therefore, it was agreed that a bi-linear (triangular) traction separation law could represent a good trade-off between good results and number of parameters to calibrate. Indeed, the main concern for the usage of Cohesive Zone Modeling in FE modeling is that accurate calibration of the adhesive's parameters is required.

For a bi-linear (triangular) traction-separation law, the initial stiffness E_0 of CZM is needed. The values of energy release rate in tension and shear (respectively G_I and G_{II}) along the fracture paths and their relative critical values (G_{Ic}) are required too, together with the cohesive strengths in tension and shear (respectively σ_n and τ_s).

These latter relate to damage initiation. They represent the end of the elastic behavior and beginning of damage. Figure 3.7 shows a schematic damage process zone and the corresponding bi-linear traction-separation law, with all the needed parameters:

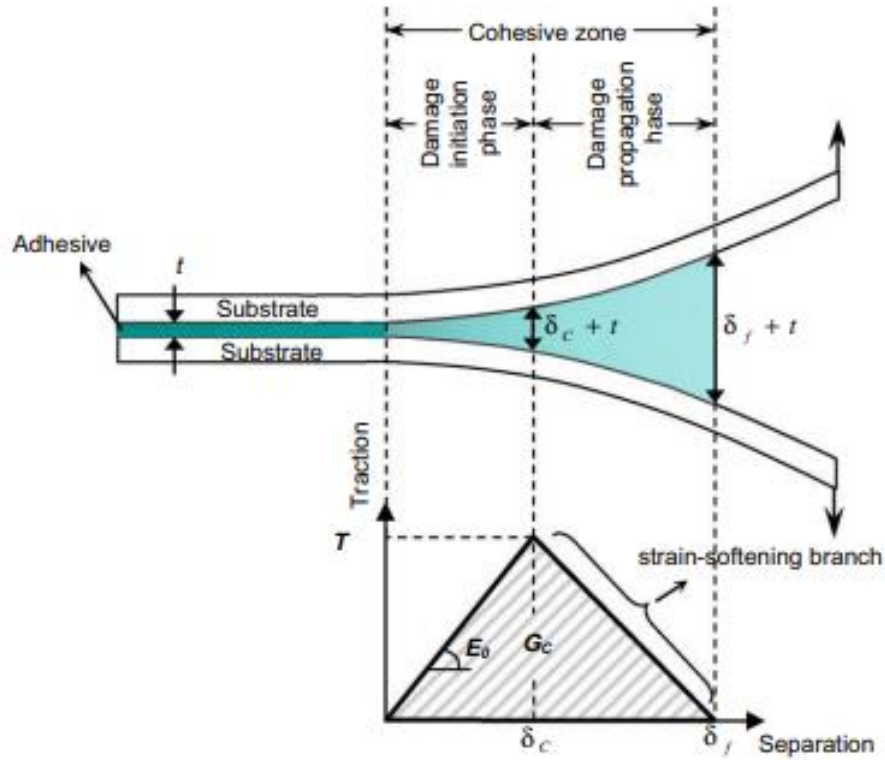


Figure 3.7: Schematic damage process zone and corresponding bi-linear traction–separation law

The fracture energy (G_{Ic} , G_{IIc}) represents the area beneath the traction–separation curve. It is the most important parameter, which is often available in literature or can be determined by means of some standard experimental tests. Actually, different techniques are nowadays available for the definition of the cohesive parameters.

The property identification technique consists on the separated calculation of each one of the cohesive law parameters by suitable tests. In this research, the inverse method has been followed. Indeed, starting from the values found in the previous study [1], the CZM parameters have been improved by iterative fitting the FE prediction with experimentally measured data (load–displacement curve), up to an accurate representation.

To simulate the failure of the adhesive, cohesive elements can replace entirely the adhesive layer or they can have minimal (or zero) thickness. Figure 3.8 shows the two different cases:

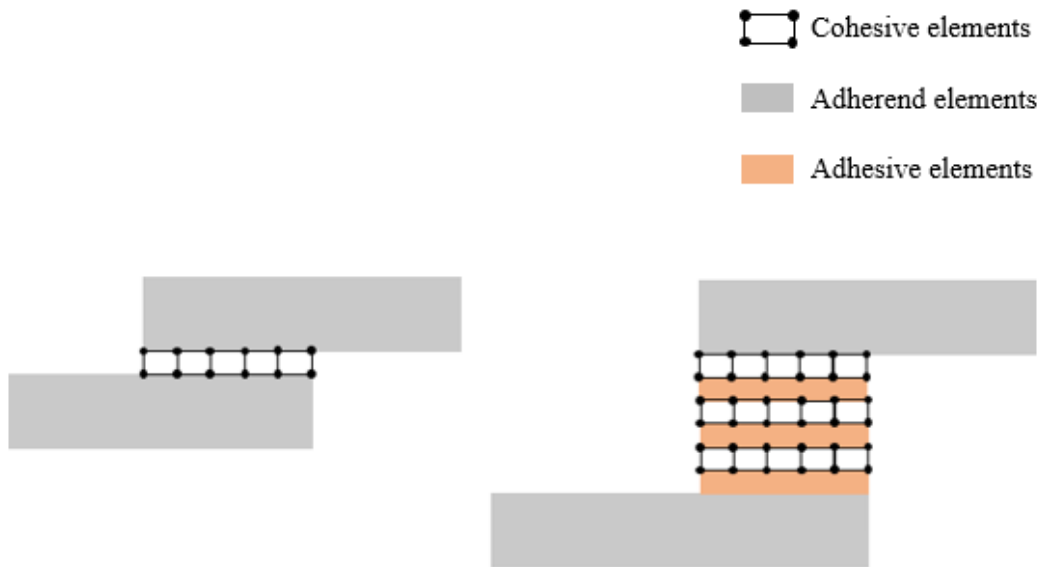


Figure 3.8: Different usage of cohesive elements

In the first case, the adhesive thickness is accounted for by the cohesive elements. The main disadvantage is that cohesive or interfacial failures are undistinguishable.

In the second cases, zero-thickness cohesive elements are used. Inserting a layer of zero-thickness cohesive elements in the middle of the adhesive allows to distinguish if the failure is interfacial or cohesive.

In this research, one layer of cohesive elements 0.5 mm thick is used to replace entirely the adhesive. Indeed, the characterization of the considered adhesive is going to be used also for industrial projects with models with bigger dimensions and a more complex geometry.

3.3 Linear Elastic Elements

A second FE model of DLJ has been built. Linear elastic C3D8I elements have been used for the adhesive, replacing the COH3D8 cohesive zone elements used in the first model.

This second model is necessary to accomplish one of the main goals of this research: to find a methodology to predict fatigue life of the adhesive. In order to achieve that, the software nCode Design Life is used. This software needs, as input, an FE model of the component whose fatigue life is going to be estimated. The issue is that nCode Design Life is not able to read cohesive elements. This is the reason why a second model was needed for this study.

The cohesive elements have been replaced with linear elastic elements, since, under fatigue loading conditions, the DLJ is loaded within its elastic limit. In this case, the Young modulus E is given as input to characterize the elastic behavior of the considered adhesive. The value of the density ρ and the Poisson's ratio ν are also provided.

CHAPTER FOUR

METHODOLOGY FOR FATIGUE LIFE PREDICTION

In this chapter, the methodology used to predict fatigue performance of adhesive joints is described. Indeed, one of the main goals of this study is to characterize the fatigue behavior of the NCA adhesive. Starting with experimentally-generated SN curves for DLJs, the objective of this research is to develop and implement a methodology to predict the fatigue behavior of the adhesive, for using in real joints with a much more complex geometry, in order to reduce the need for fatigue testing, which is often expensive and time consuming. In order to achieve that goal, nCode Design Life is used in this study.

4.1 Procedure in nCode Design Life

nCode DesignLife is a design tool that identifies critical locations and is able to rapidly calculate realistic and accurate fatigue lives from leading FE results for different materials.

To perform the analysis, at least three glyphs are needed: the Solver glyph, the Input glyph and the Display or Output glyph. For what concerns the solver, among the several methods and analysis that nCode Design Life offers, for this research the Stress-Life (SN) method has been chosen. Its primary application is high-cycle fatigue, where nominal stress controls the fatigue life.

Concerning the inputs, in order to perform the analysis, nCode DesignLife requires the FE results of the model, information about the load and SN curves of the materials used for the component.

As already explained in Chapter three, the FE model used to get FE results is the one using linear elastic elements for the adhesive, since nCode Design Life is not able to work with cohesive elements.

The load in the nCode simulations is a constant amplitude load. The maximum and minimum loads correspond exactly to the ones that have been applied to the DLJs in the experimental tests. In this way, a direct comparison to discuss the accuracy of the prediction will be possible.

For what concerns the material, a wide range of methods is provided for defining the SN curves, including the ability to interpolate multiple material data curves for factors such as mean stress or stress ratio. A default database with fatigue properties for many commonly used materials is also provided. Indeed, for the adherends, an aluminum alloy present in the database has been selected. For the adhesive, the standard SN material model has been used. This model allows to define a SN curve for the considered adhesive by setting different material properties and parameters. Some of these must be obtained using the curves obtained experimentally.

Concerning the output, the FE Display glyph has been chosen. This displays the FE model and the associated FE results or the CAE fatigue results (life or damage).

Before running the analysis all the glyphs (input, solver, output) present in the workspace must be connected to each other. Once this has been done, it is possible to run the simulation.

4.1.1 Material properties and parameters

Some of the material properties and parameters requested by the software nCode must be obtained exploiting the curves of the experimental tests. These parameters are:

- SRI1 - Stress range intercept [MPa]
- b1 - First fatigue strength exponent
- Nc1 - Fatigue transition point [cycles]
- b2 - Second fatigue strength exponent
- RR - R-ratio of Test
- SE - Standard Error

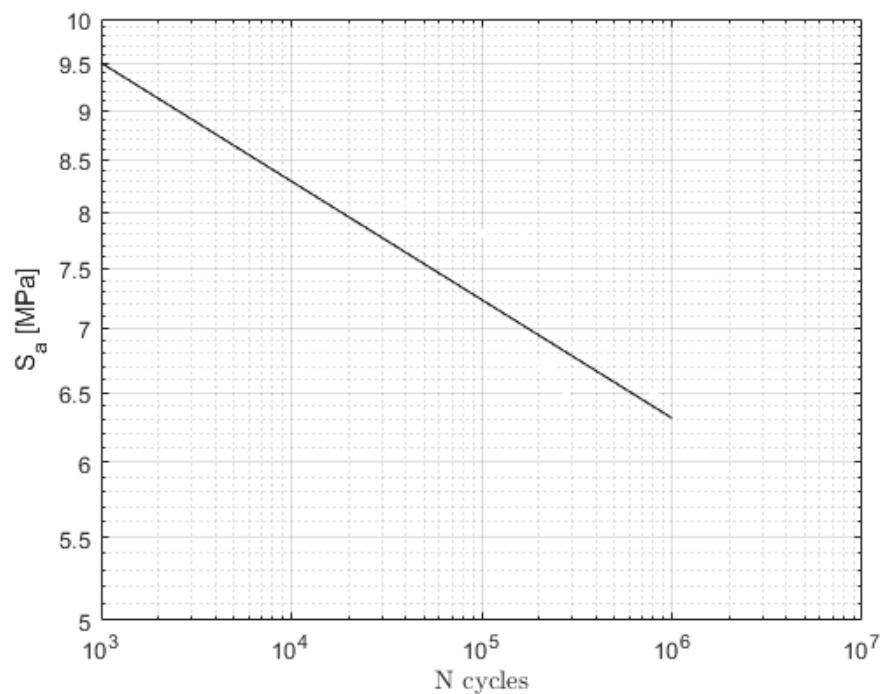


Figure 4.1: Schematic of a High-Cycle Fatigue Curve (SN) of Ferritic Metals

SRI1, together with b_1 , define the intercept and the slope of the main SN curve. To obtain these values from the experimental data, fatigue data points must be plotted on log-log scales diagram. Equation (1) represents the relationship between the fatigue strength S vs. fatigue life N . The parameter b_1 represents the slope of the SN line (Fig.4.1).

$$\ln(y) = b_1 \cdot \ln(x) + c \quad (1)$$

For what concerns the quantity SRI1, represents the stress range when the number of cycles to failure is equal to 1 cycle. In order to obtain it, the value of the maximum allowable alternating stress at 10^6 cycles S_2 and the value of the slope b_1 are needed. In order to obtain the maximum allowable alternating stress at 10^6 cycles S_2 , the maximum allowable alternating load $F_{a,2}$ at 10^6 cycles is needed. This value can be read on the graph, exploiting the linear regression analysis. Once that the maximum allowable alternating load $F_{a,2}$ at 10^6 cycles is known, FE static simulation is required in order to get the corresponding stress. From the FE simulation in Abaqus, the element with the highest (Von Mises) stress, when a certain load is applied, can be identified. The ratio between the highest (Von Mises) stress tolerated by that element and the applied load must be calculated. Since the loads applied during the fatigue tests operate in the elastic range, the stress/load ratio will not change. Therefore, knowing this ratio and the maximum allowable alternating load at 10^6 cycles $F_{a,2}$, the maximum allowable alternating stress at 10^6 cycles S_2 is obtained.

Finally, the Eq.2 to evaluate SRI1 (range intercept at 1 cycle) is shown below:

$$SRI1 = \frac{2 \cdot S_2}{(10^6)^{b_1}} \quad (2)$$

For what concerns the other parameters, N_{c1} is the fatigue transition point of the material. It changes with the material, but generally it is equal to 10^6 cycles. The parameter b_2 represents the slope of the SN curve at lives higher than N_{c1} . If set to zero, this represents a fatigue limit. If no particular change in slope is required, then it should be the same as b_1 (approach often used for welds). RR is the stress ratio of the constant amplitude fatigue tests done and it is defined as the ratio between maximum and minimum stress applied during the fatigue cycle.

Concerning the value of the Standard Error of $\text{Log}(N)$, this is equal to:

$$SE = \frac{\sigma}{\sqrt{n}} \quad (3)$$

where σ is the standard deviation and n is the number of samples. In this study, a value of SE has been calculated for each set of points corresponding to different loads and an average value of the three is used in nCode Design Life.

4.2 Mesh sensitivity analysis

In this research, a sensitivity analysis has been carried on in order to investigate the effect of the increased discretization on the accuracy of the results. The linear elastic model considered 2 mm C3D8I elements for the adherends and different mesh sizes and element thickness for the adhesive.

Indeed, to investigate how much the converged solution changes refining the adhesive mesh size, 2 mm, 1 mm and 0.5 mm C3D8I elements are considered. The element thickness is kept constant and equal to 0.5 mm. Therefore, being the adhesive thickness of the joints equal to 0.5 mm, only one layer of linear elastic elements is needed to represent the adhesive.

To study the effect of the element thickness on the results, the mesh size is kept constant and equal to 0.5 mm, while the element thickness varies from 0.5 mm to 0.25 mm. In this case, two layers of linear elastic elements are needed in order to replace the adhesive. It has been decided to reduce the thickness of the elements with a mesh size equal to 0.5x0.5mm, in order to have a length-to-thickness ratio equal to 2, at maximum.

CHAPTER FIVE

RESULTS AND DISCUSSION

Results are shown and discussed in this chapter. Firstly, the results of the static and fatigue experimental tests on steel SLJs are shown, in order to discuss the effect of material manufacturing and surface roughness on the static and fatigue performance of the joints.

Secondly, the outcomes of the static and fatigue experimental tests on aluminum DLJs are presented. These are compared with the results coming from the FE analysis, in order to discuss the accuracy of the models that have been built and the methodology to predict fatigue life of the joints.

5.1 Experimental testing results

5.1.1 Single Lap Joints

This study can be divided in two main parts. In the first part, an experimental plan involving Single Lap Joints has been designed. The purpose of the experiments for the SLJs is to assess the influence of the material manufacturing on the fatigue strength of the joints, while the other key design variables, such as adhesive thickness and overlap length, remain constant. To assess the influence of material manufacturing on the fatigue performance of SLJs, three levels of alternating load have been investigated, while the mean load is kept constant. In order to assess its influence on the mechanical behavior of the joints, two levels of mean load have been studied: 30% and 45% of the average ultimate load of the considered configuration. The frequency is set equal to 10 Hz.

A third configuration of SLJs has been prepared, in order to investigate the influence of the surface roughness on the fatigue life when the material manufacturing is the same. The substrates of Configuration 3 are made with wrought stainless steel, as the ones of Configuration 2, but they have been prepared such to have a significant difference in the surface roughness. For what concerns the Configuration 2, the Average Surface Roughness R_a is roughly 500 nm. For Configuration 3, the value of average surface roughness of the substrates decreases significantly, being between 50 nm and 100 nm. These values have been obtained using the WYKO NT1100 optical profiler system.

From the static tests for the SLJs the shear strength of the adhesive can be assessed, from the fatigue tests SN curves are obtained for each considered configuration. Also in this case, before analyzing the outcomes of the static and fatigue tests, the first thing to observe is the failure mode of the adhesive.

Adhesively bonded joints may fail adhesively or cohesively. Adhesive failure is interfacial between the adhesive and the adherend, while cohesive failure occurs entirely within the adhesive layer itself with adhesive layers remaining bonded to both substrate surfaces. The ideal mode of failure is a 100% cohesive failure within the adhesive layer, which allows maximum strength of the adhesive to be reached. Adhesive or mixed mode (partially cohesive and partially adhesive) failures can happen when the surface preparation is not appropriate to bond the substrates. For all the static and fatigue tests done, the Double Lap Joints showed a cohesive failure mode.

5.1.1.1 Effect of substrate manufacturing

5.1.1.1.1 Static Strength (Baseline)

This section discusses the baseline static strength of Single Lap Joints and the effect of substrate manufacturing method. For each configuration of SLJs, quasi-static shear-tensile tests have been performed. In Figures 5.1 and 5.2 are reported respectively the load-displacement curves for Configuration 1 (AM-AM) and Configuration 2 (WR-WR). The curves have been post-processed with MATLAB, using a filter to lower the effect of noise of the measurements. When considering the wrought configuration (Configuration 2) the average failure load increases of about 2.11% with respect to the additive configuration (Configuration 1).

Table 5.1 summarizes the obtained results for the failure loads. In order to have a visual impact of the obtained results, Fig.5.3 and Fig. 5.4 show the baseline static test results of Single Lap Joints. The average failure load of wrought configuration (Configuration 2) is only 2.11% higher than additive configuration (Configuration 1). Figure 5.4 shows the average shear strength of the adhesive for each configuration with the respective standard deviations. The values have been obtained normalizing the failure load by the bonding area of each sample. An average is done.

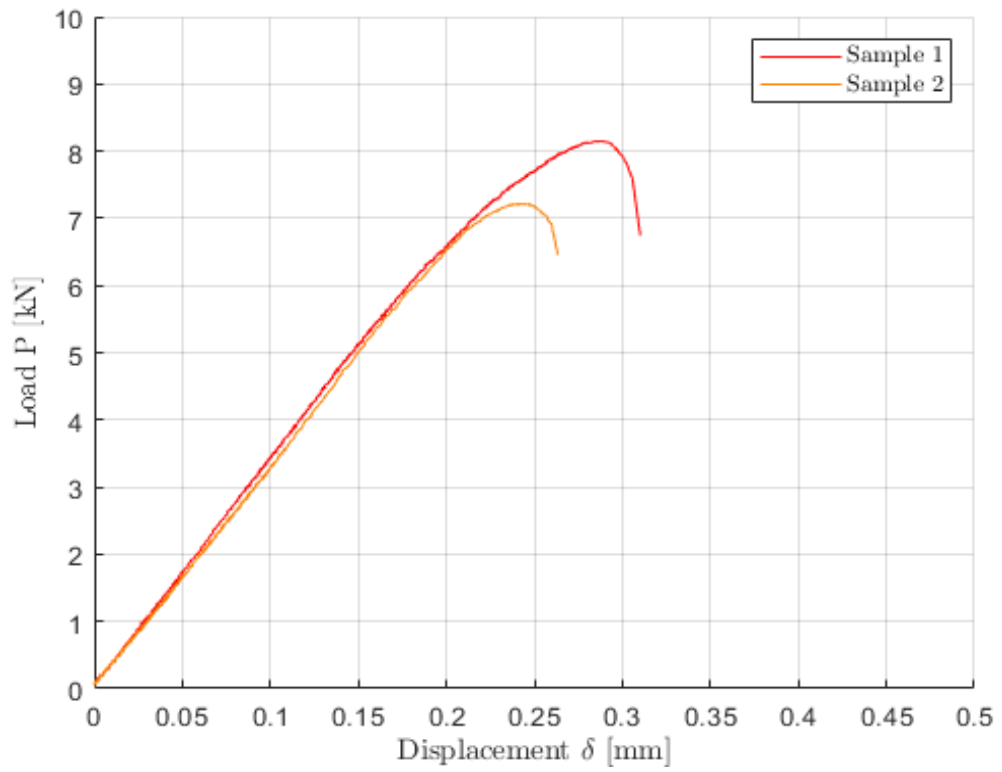


Figure 5.1: Sample Load-Displacement Data for AM-AM Joints

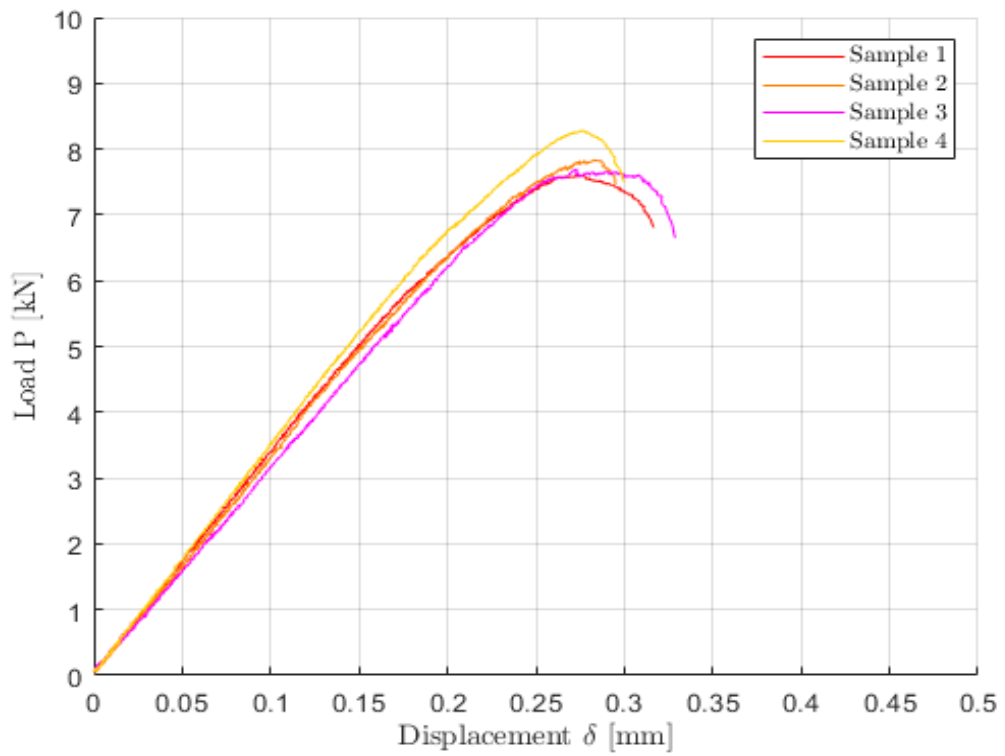


Figure 5.2: Sample Load-Displacement Data for WR-WR Joints

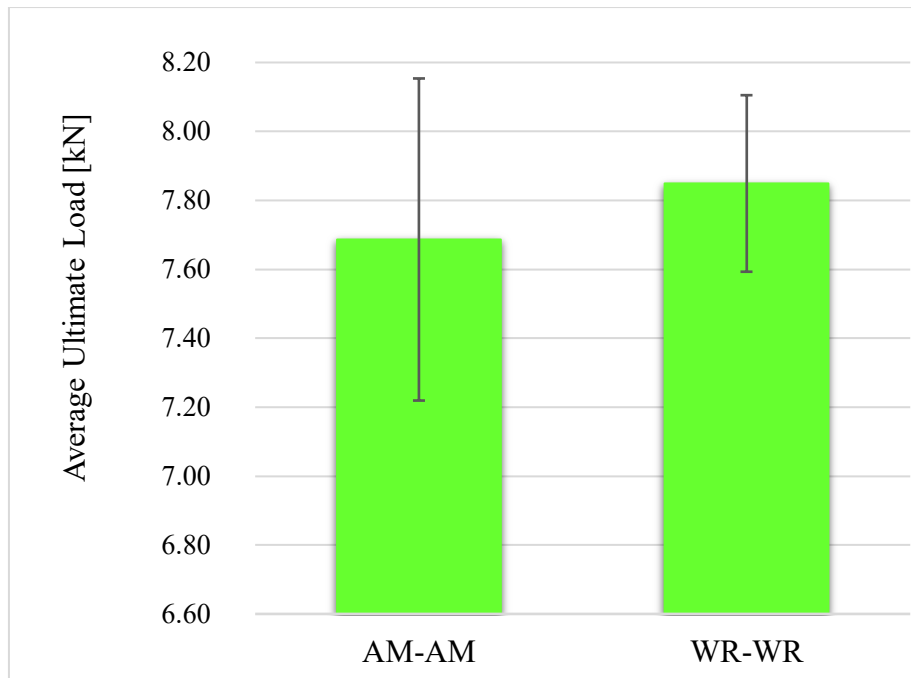


Figure 5.3: Average Ultimate Load for the two configurations of Single Lap Joints

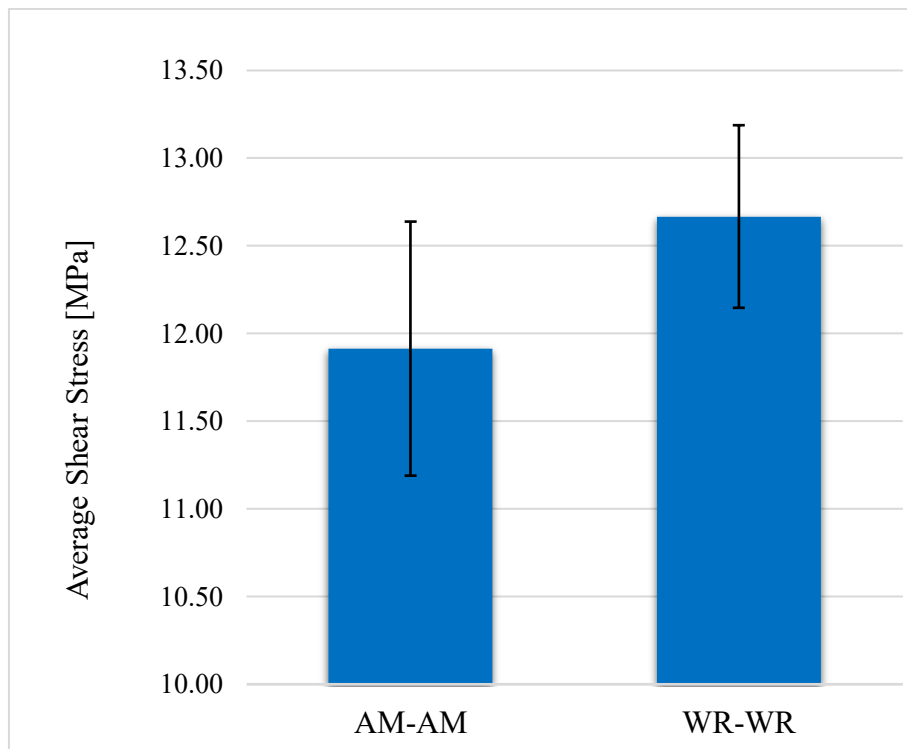


Figure 5.4: Average Shear Stress for the two configurations of Single Lap Joints

As expected from the trend of the average ultimate load, the average shear stress of wrought configuration is higher than additive configuration. The standard deviation for Configuration 1 (AM-AM) is higher. More dispersion is present.

Table 5.1: Effect of material manufacturing on Ultimate Failure Load of Single Lap Joints

Ultimate Failure Loads [kN]							
Configuration	Substrates material manufacturing	Sample number				Average	Standard Deviation
		1	2	3	4		
1	AM-AM	8.15	7.22	-	-	7.69	0.47
2	WR-WR	7.60	7.84	7.69	8.28	7.85	0.26

Looking at the surfaces of the SLJs after the failure, it is possible to notice that for both Configuration 1 and Configuration 2 the failure mode is always cohesive.

5.1.1.1.2 Fatigue Performance

This section discusses the effect of substrate manufacturing method on Single Lap Joints fatigue performance.

In order to assess the influence of substrate manufacturing method on the fatigue performance of SLJs, three levels of alternating load have been investigated, while the mean load is kept constant. Two values of mean load have been studied: 30% and 45% of the average ultimate load of the considered configuration. The frequency is set equal to 10 Hz.

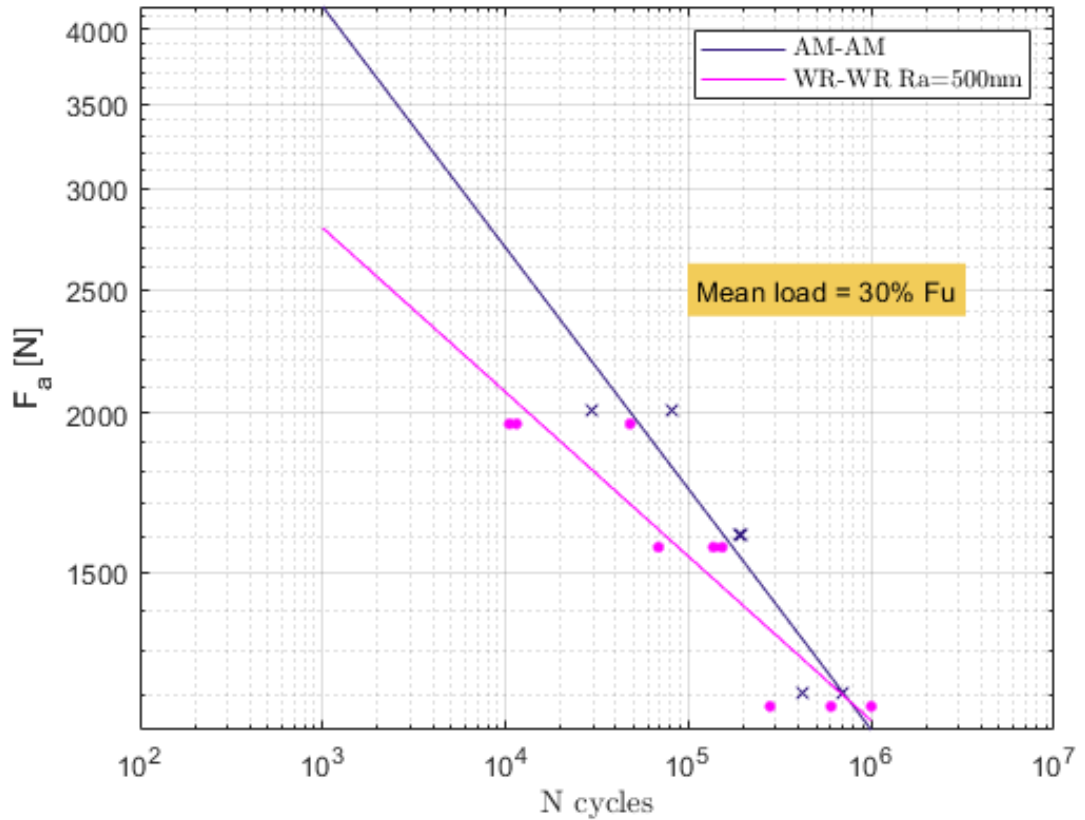


Figure 5.5: Fatigue performance of Single Lap Joints with AM vs. wrought substrates – Mean load=30% F_u

Figure 5.5 shows the alternating load F_a as percentage of the average static ultimate load F_u versus the number of cycles to failure, for Configuration 1 (AM-AM) and Configuration 2 (WR-WR) when a mean load equal to 30% of the average ultimate load F_u is applied. Both the load and number of cycles are displayed on logarithmic scales.

Configuration 1 (AM-AM) shows a better performance up to 500,000 cycles. Indeed, when the same alternating load (as percentage of the average ultimate load) is applied, the Single Lap Joints made with 3D printed and extruded substrates have a longer life (number of cycles). For lower loads the trend is the opposite. Configuration 2 (WR-WR) is the one that, under the same alternating load, is able to last more cycles.

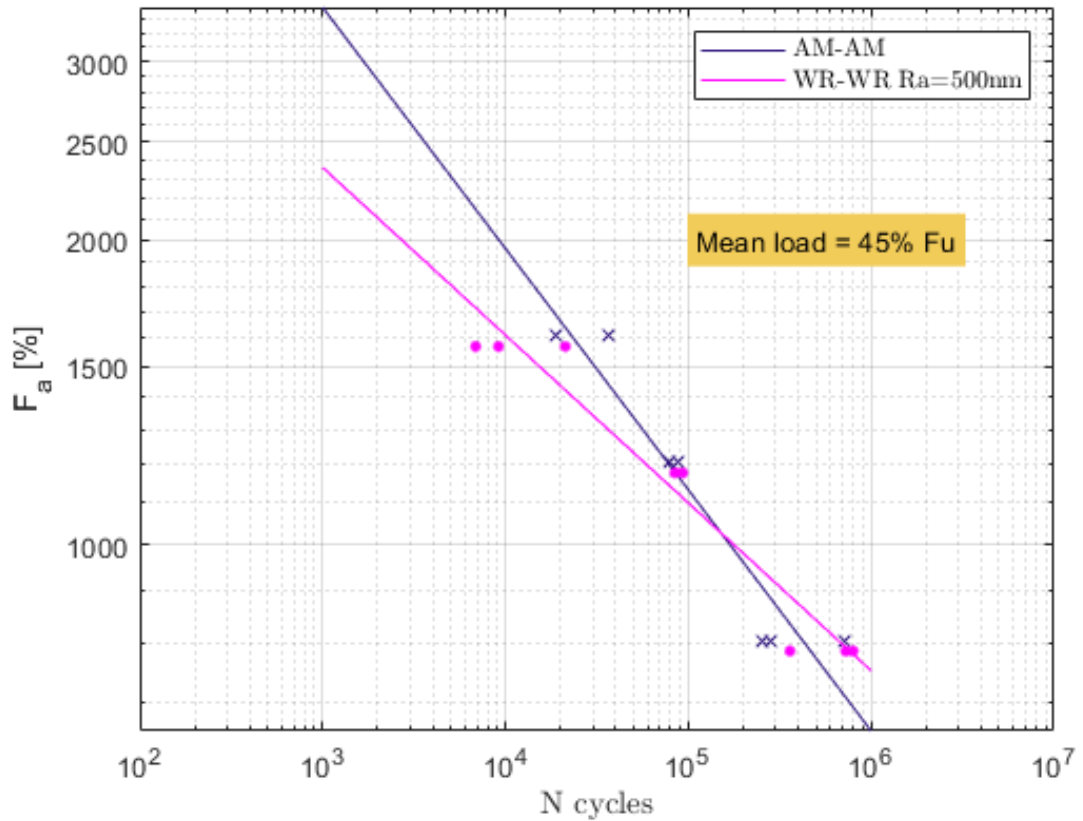


Figure 5.6: Fatigue performance of Single Lap Joints with AM vs. wrought substrates – Mean load=45% Fu

Figure 5.6 shows that, when changing the value of the mean load, the behavior is the same. Indeed, when higher loads are applied, Configuration 1 (AM-AM) shows a better performance, since it is able to last more cycles. Under lower loads, the SLJs of Configuration 2 (WR-WR) last more. The number of cycles at which the trend switches in this case is roughly 100,000 cycles.

In all the tests that have been performed, the failure mode is cohesive, without differences between Configuration 1 (AM-AM) and Configuration 2 (WR-WR).

5.1.1.2 Effect of Surface Roughness

In this section, the effect of the substrates' Average Surface Roughness on the static and fatigue performance of the joints is discussed.

The Surface Roughness may be a significant variable affecting the mechanical behavior of Single Lap Joint. Increasing the surface roughness and the asperities of the material can encourage the mechanical interlocking of the adhesive, improving the strength of the joint. In this study, in order to investigate this aspect, two configurations of SLJs made with wrought stainless steel are tested.

The substrates have been prepared such to have a significant difference in the surface roughness. For Configuration 2, the average surface roughness measured for the substrates is roughly 500 nm. For Configuration 3, the value of average surface roughness of the substrates decreases significantly, being between 50 nm and 100 nm. These values have been obtained using the WYKO NT1100 optical profiler system.

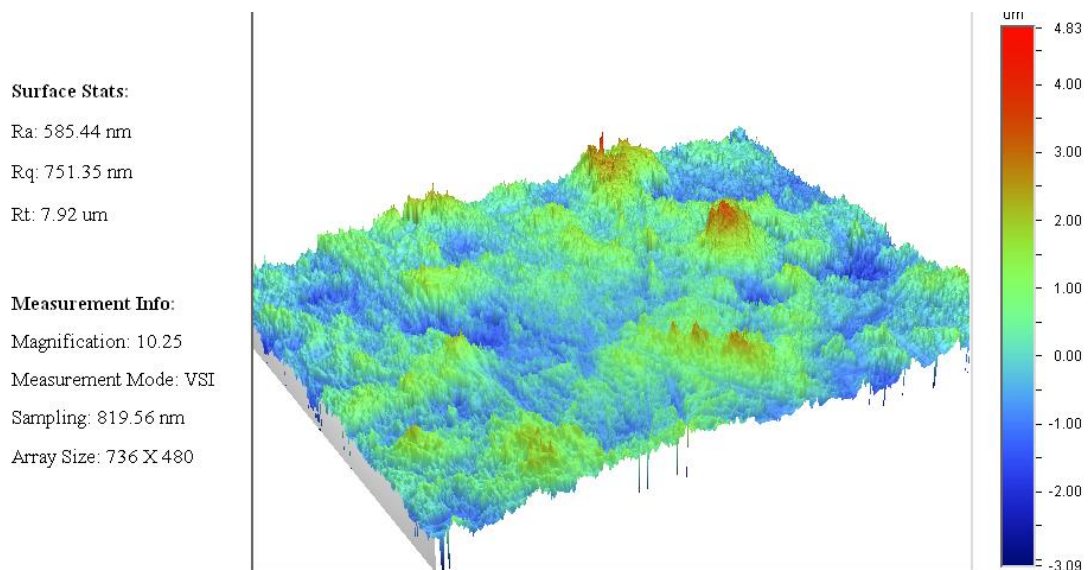


Figure 5.7: 3D surface measurement for wrought substrate with higher surface roughness

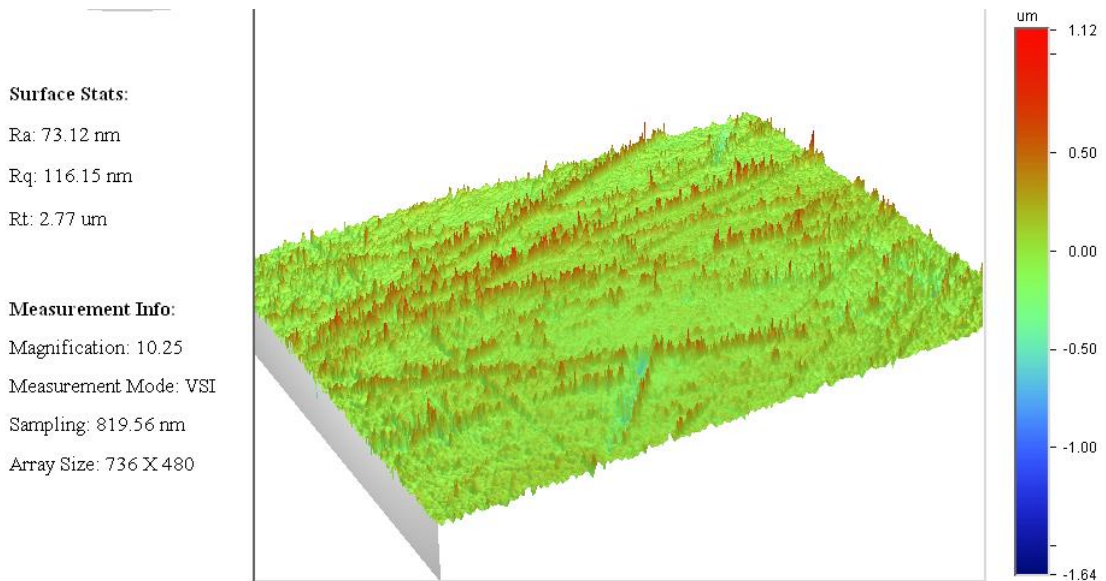


Figure 5.8: 3D surface measurement for wrought substrate with lower surface roughness

In Figures 5.7 and 5.8, the images show a 3D measurement of the surface of two wrought substrates, representing respectively Configuration 2 and Configuration 3.

5.1.1.2.1 Static Strength (Baseline)

This section discusses the effect of average surface roughness on the baseline static strength of Single Lap Joints. For each configuration, four quasi-static shear-tensile tests have been repeated in order to obtain more robust results from a statistical point of view: the reported standard deviations of the samples are very low and this is an indication of the good reliability of the results. In Fig.5.9 and 5.10 report respectively the SLJ tested with surface roughness equal to 500 nm (Configuration 2) and 100 nm (Configuration 3). Also in this case, the curves have been post-processed with MATLAB, using a filter to lower the effect of noise of the measurements. When considering the lowest surface roughness (100 nm) the failure load is 6.5% higher than Configuration 2.

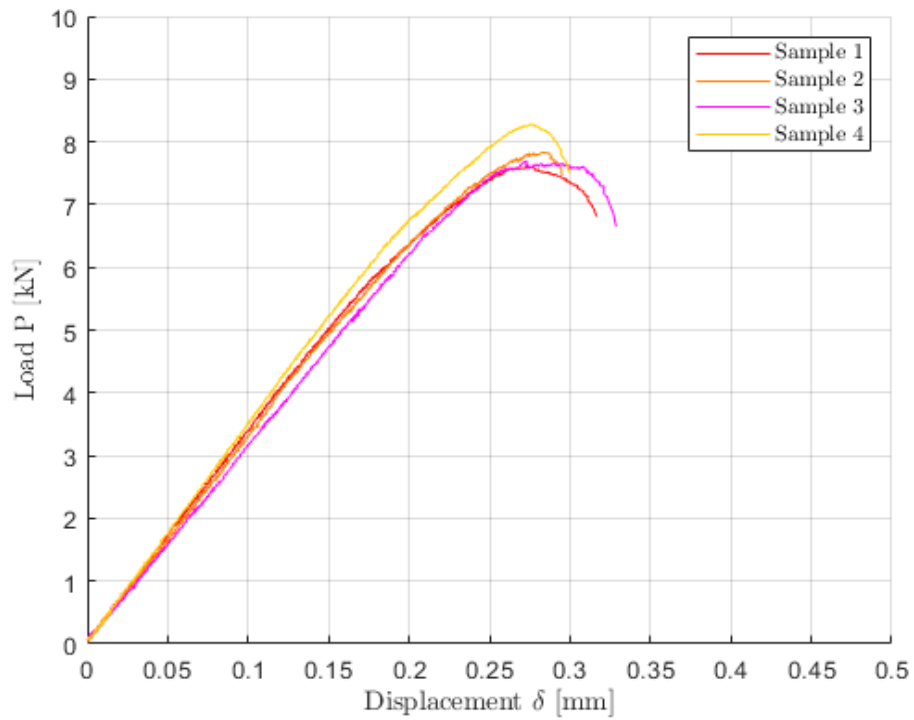


Figure 5.9: Sample Load-Displacement Data for SLJ made with wrought substrates with higher surface roughness

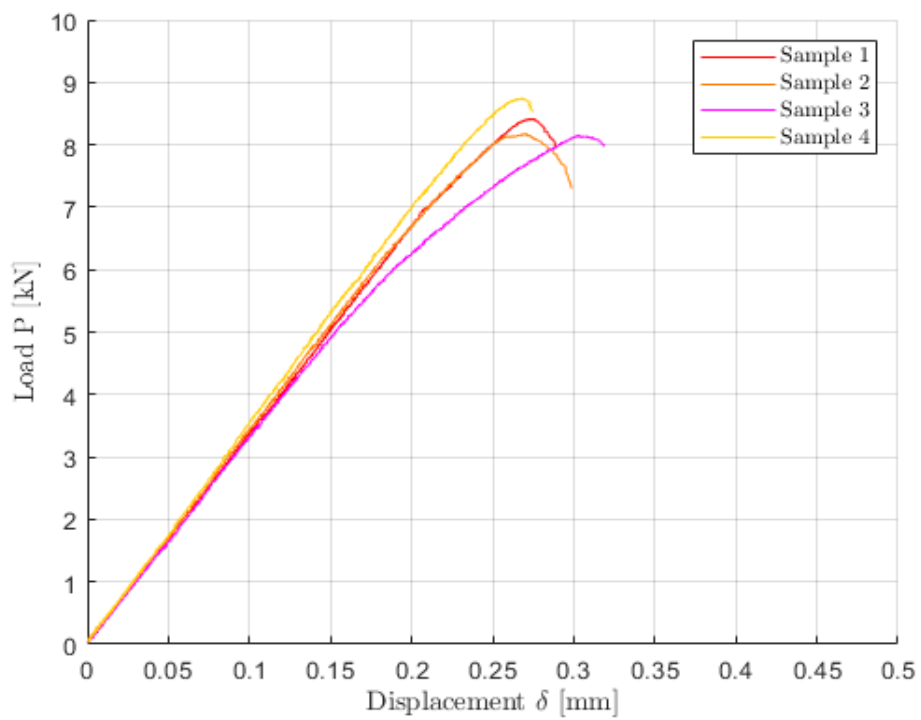


Figure 5.10: Sample Load-Displacement Data for SLJ made with wrought substrates with lower surface roughness

Looking at the surfaces of the SLJs after the failure, both Configuration 2 and Configuration 3 show a cohesive failure mode. Table 5.2 summarizes the obtained results for the failure loads. Figure 5.11 shows bar charts of the failure loads with the respective standard deviations. When decreasing the surface roughness, the failure loads increases. Figure 5.12 reports the average shear strength of the adhesive for each configuration with the respective standard deviations. The values have been obtained normalizing the failure load by the bonding area of each sample. An average is done.

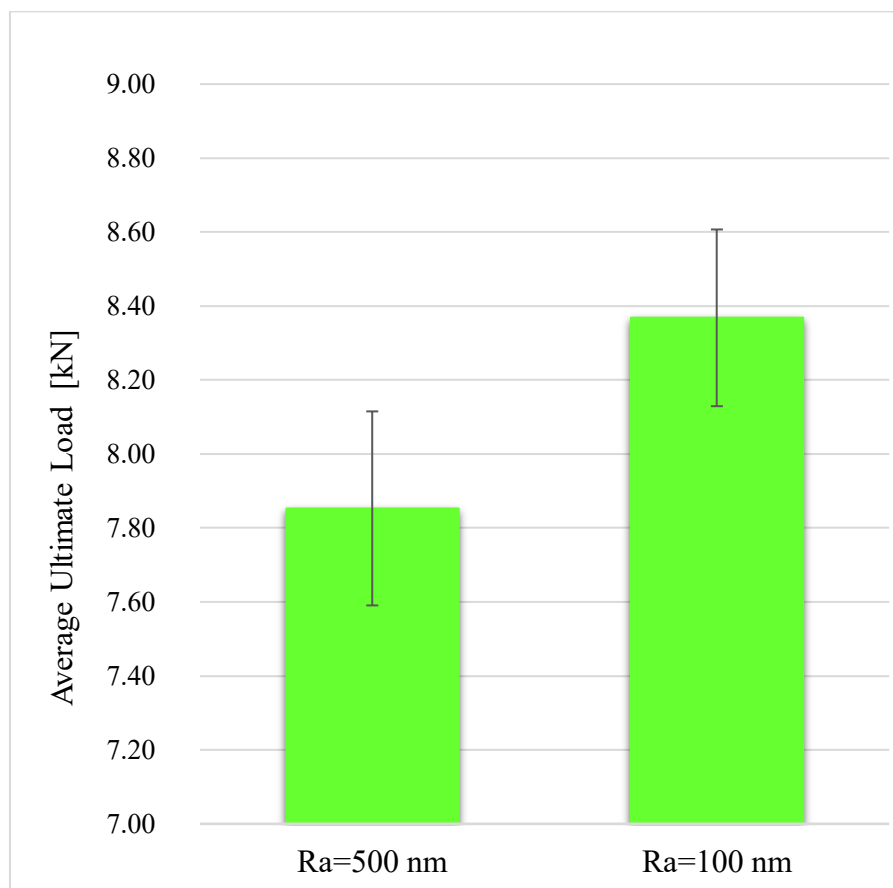


Figure 5.11: Average Ultimate Load for the two configurations of Single Lap Joints

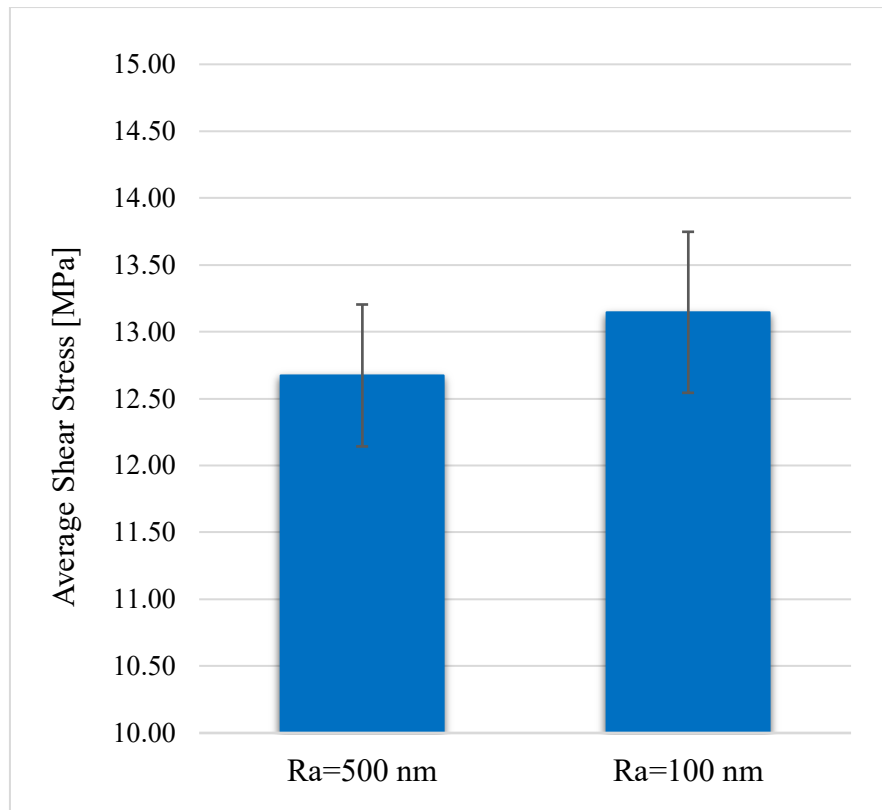


Figure 5.12: Average Shear Stress for the two configurations of Single Lap Joints

Table 5.2: Effect of Surface Roughness on Ultimate Failure Load of Single Lap Joints

Configuration	Average surface roughness R_a [nm]	Ultimate Failure Load [kN]				Average [kN]	Standard Deviation [kN]
		1	2	3	4		
WR-WR	500	7.60	7.84	7.69	8.28	7.85	0.26
WR-WR	50÷100	8.41	8.17	8.14	8.74	8.37	0.24

5.1.1.2.2 Fatigue Performance

This section discusses the effect of surface roughness on fatigue performance of wrought Single Lap Joints.

In order to assess the influence of the surface roughness on the fatigue performance of SLJs, one value of mean load and three levels of alternating load have been investigated. For each configuration, in order to obtain a more reliable SN curve, 3 repetitions have been performed for each point. Figure 5.13 shows the alternating load F_a versus fatigue life N , for both the configurations of Single Lap Joints. The mean load applied is equal to 45% of the Average Ultimate Load F_u of each considered configuration.

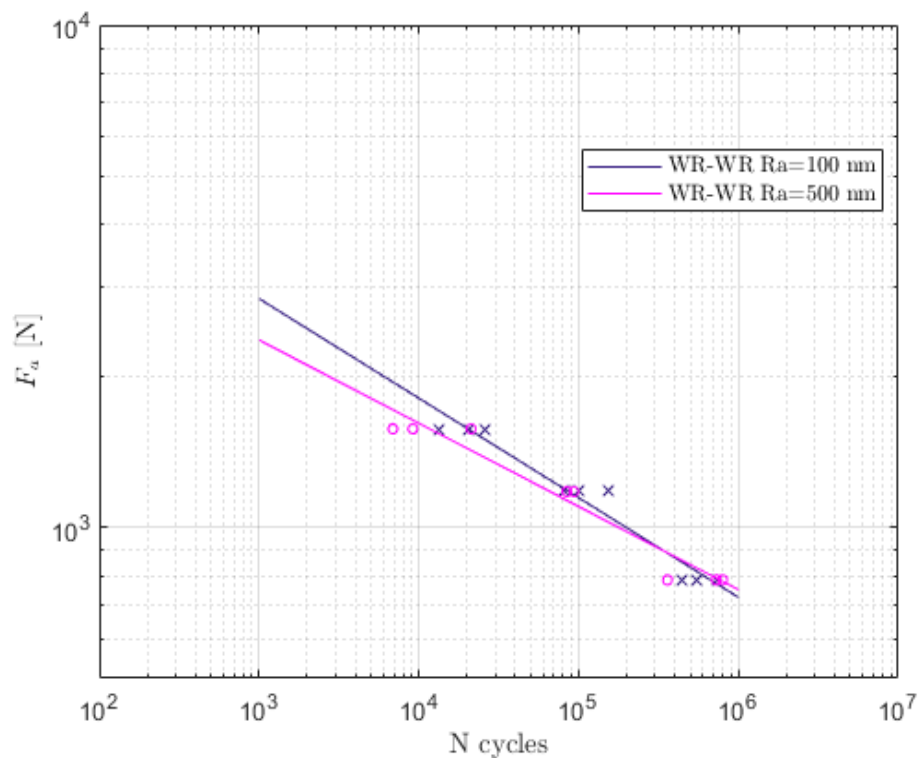


Figure 5.13: Effect of Surface Roughness on fatigue performance of Single Lap Joints
Up to a number of cycles equal to 300000, Configuration 3 (Ra=100 nm) shows a better performance. When the same alternating load is applied, the Single Lap Joints with a lower surface roughness have a longer fatigue life (number of cycles). After

300000, the trend is the opposite. Applying the same alternating load, Configuration 2 shows a higher fatigue life.

The fatigue performance of the joints with a lower roughness (Configuration 3) decreases due to the shift in failure mode after 300000 cycles. Indeed, looking at the surfaces of the SLJs after the failure, for Configuration 2 the failure mode is always cohesive (Fig.5.14). However, for Configuration 3, it switches from cohesive to mixed (adhesive and cohesive) when the number of cycles is higher than 300000, as shown in Fig.5.15.

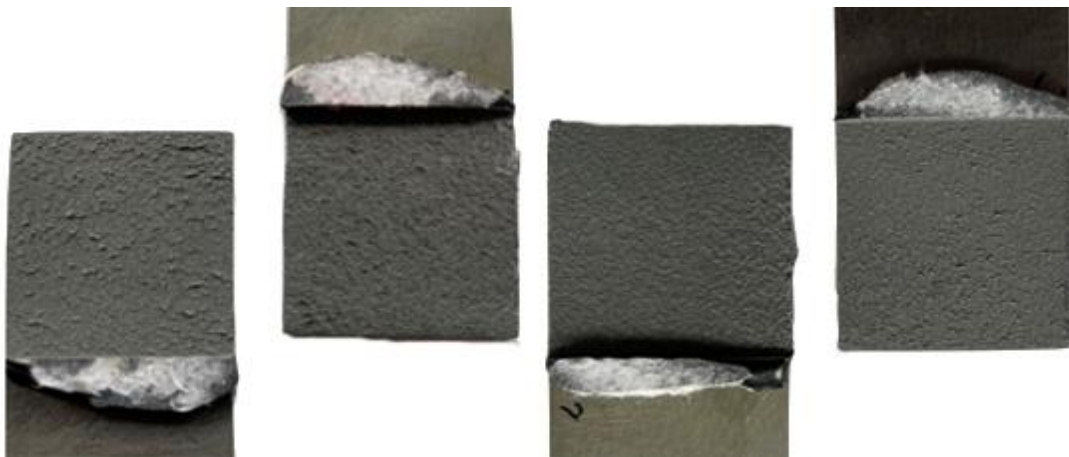


Figure 5.14: Fracture Surface for Configuration 2 before (left) and after (right) 300000 cycles

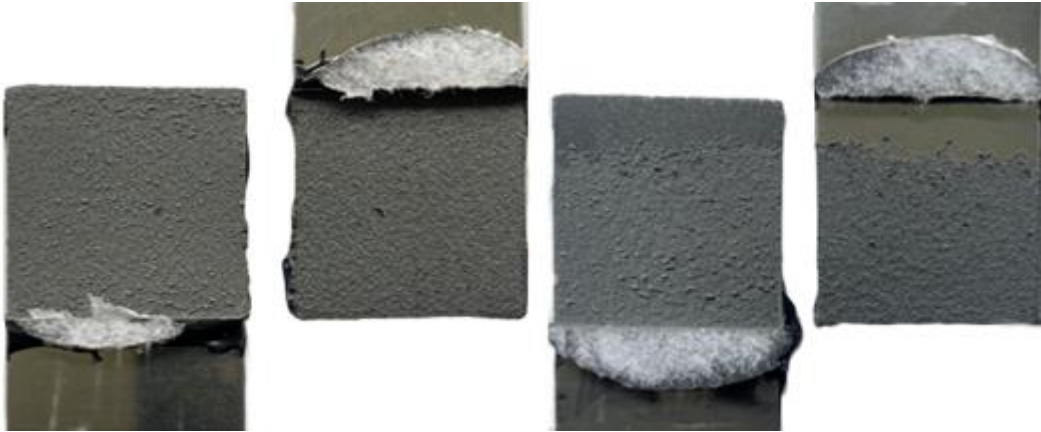


Figure 5.15: Fracture Surface for Configuration 3 before (left) and after (right) 300000 cycles

5.1.2 Double Lap Joints

In the second part of the research, in order to properly parametrize the non-commercially available epoxy-based adhesive used in this research, an experimental plan involving Double Lap Joints has been designed. The purpose of the experiments for the DLJs is to assess the influence of the material manufacturing on the fatigue strength of the joints, while the other key design variables, such as adhesive thickness and overlap length, remain constant. The main output of the static tests for the DLJs is the shear strength of the adhesive, while from the fatigue tests SN curves are obtained for each considered configuration: this parameter is crucial for the development of a methodology for fatigue life prediction using finite element modelling.

5.1.2.1 Static Strength (Baseline)

This section discusses the baseline static strength of Double Lap Joints and the effect of substrate manufacturing method.

For each configuration of DLJs, four quasi-static shear-tensile tests have been repeated in order to obtain more robust results from a statistical point of view. In

Figures 5.16 and 5.17 are reported respectively the load-displacement curves for Configuration 1 (AM-AM-AM) and Configuration 2 (AM-EX-AM). The curves have been post-processed with MATLAB, using a filter to lower the effect of noise of the measurements. Table 5.3 summarizes the obtained results for failure loads.

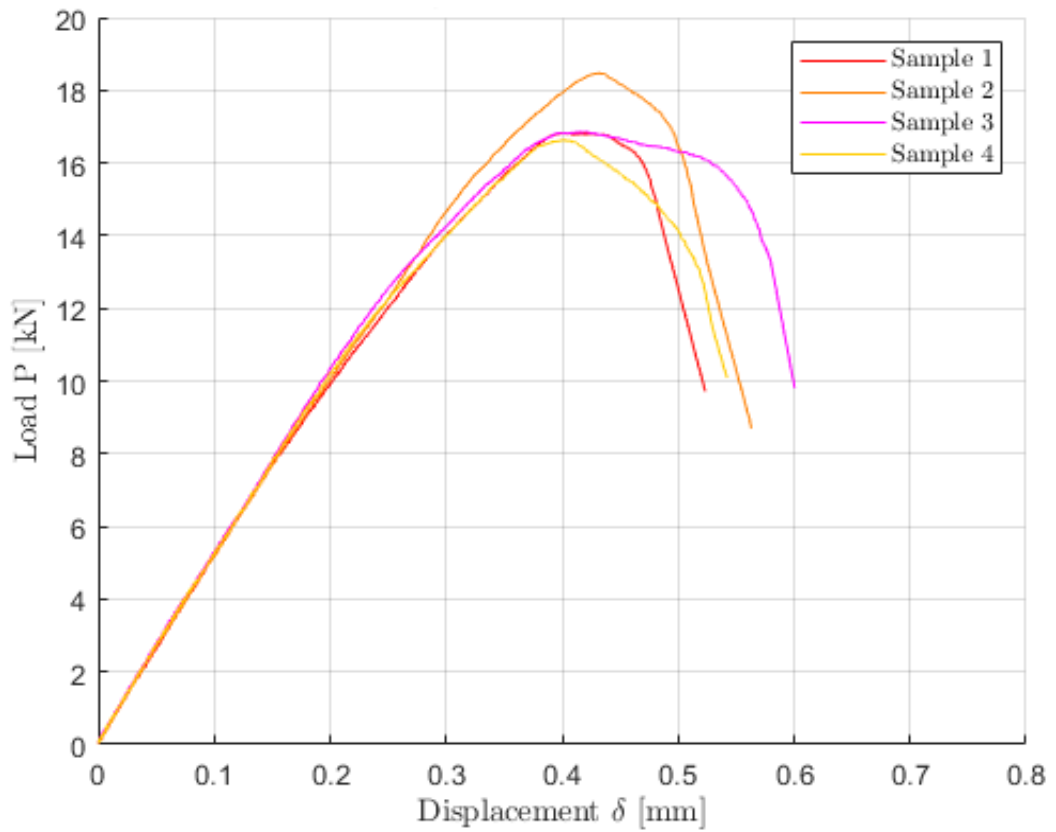


Figure 5.16: Sample Load-Displacement Data for AM-AM-AM joints

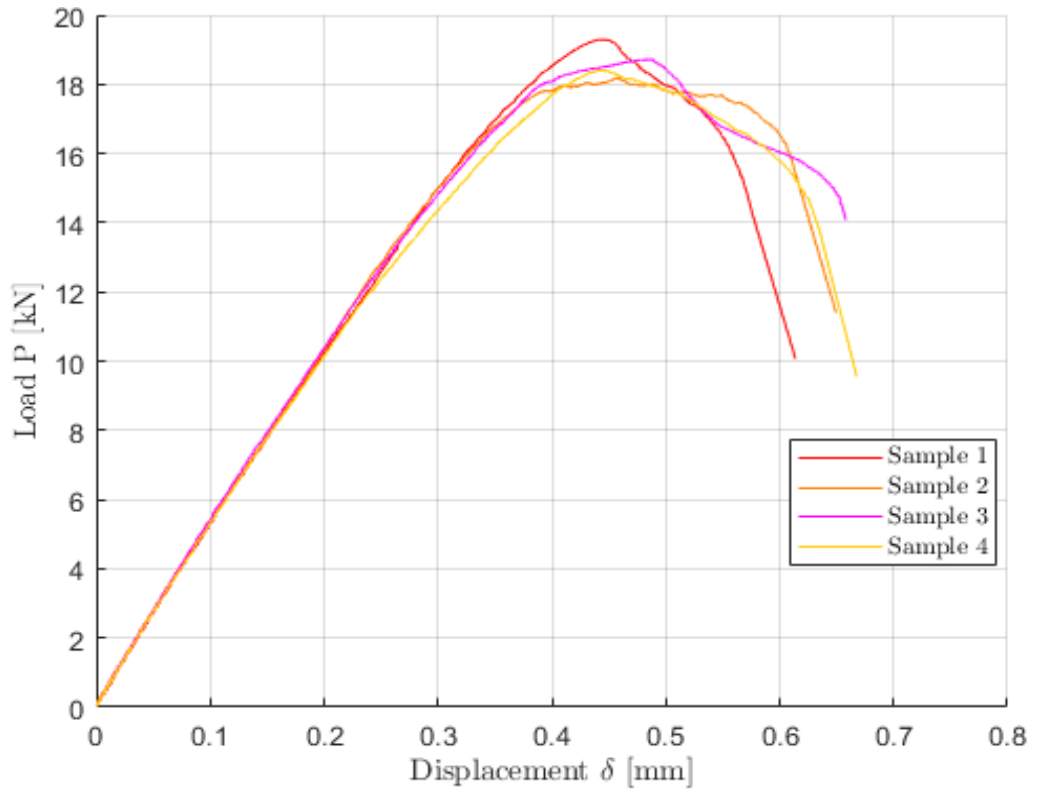


Figure 5.17: Sample Load-Displacement Data for AM-EX-AM joints

Table 5.3: Effect of material manufacturing on Ultimate Failure Load of Double Lap Joints

Configuration	Substrates material manufacturing	Ultimate Failure Load [kN]				Average [kN]	Standard Deviation [kN]
		1	2	3	4		
1	AM-AM-AM	16.82	18.47	16.86	16.63	17.19	0.74
2	AM-EX-AM	19.29	18.19	18.72	18.40	18.65	0.41

Figure 5.18 shows bar charts of the failure loads with the respective standard deviations. Figure 5.19 shows the average shear strength of the adhesive for each

configuration. The values have been obtained normalizing the failure load by the bonding area of each sample. An average is done.

The average failure load for AM-EX-AM configuration (Configuration 2) is about 8.48% with respect to the AM-AM-AM configuration (Configuration 1). As the ultimate load trend, the average shear stress is higher in AM-EX-AM configuration (Configuration 2). The standard deviation is higher for Configuration 1 (AM-AM-AM), as happened with the SLJs. The joints made only with 3D printed substrates show a greater dispersion.

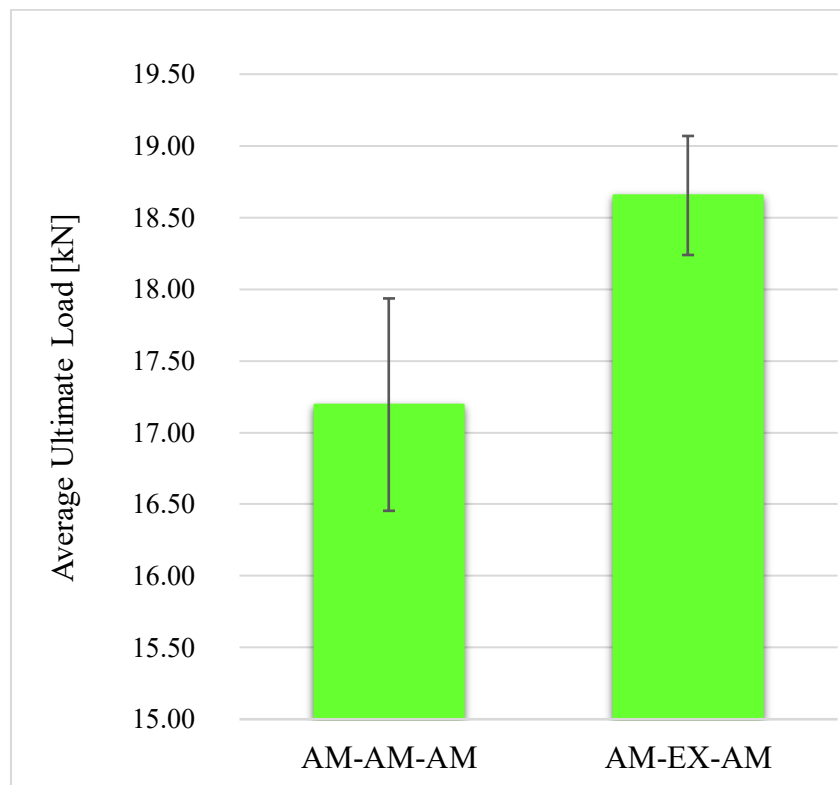


Figure 5.18: Average Ultimate Load for the two configurations of Double Lap Joints

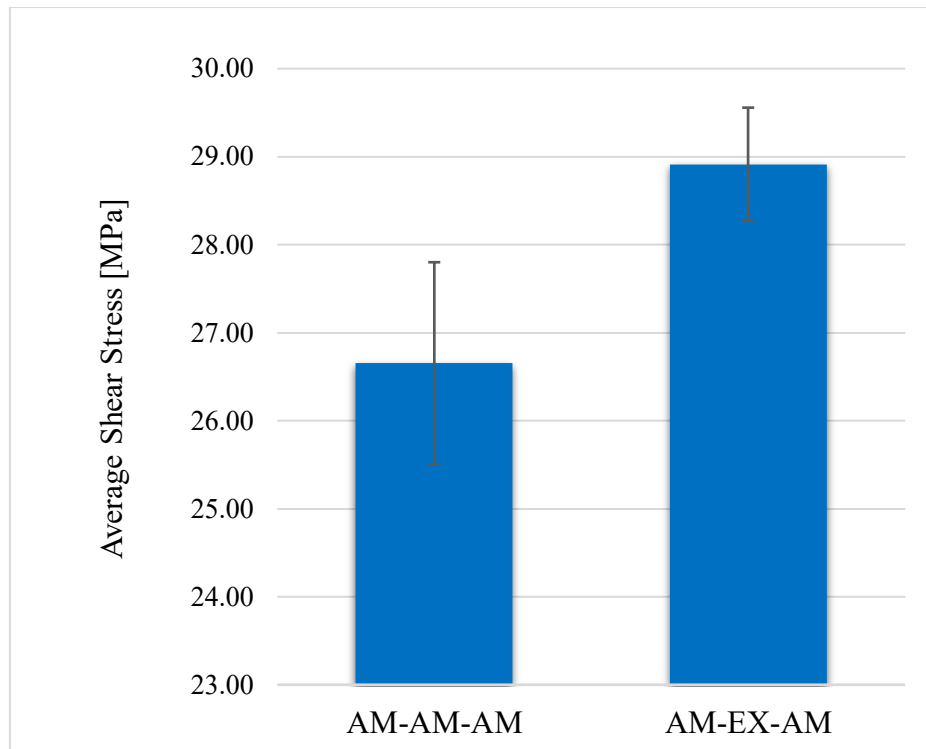


Figure 5.19: Average Shear Stress for the two configurations of Double Lap Joints

Looking at the surfaces of the DLJs after the failure, it is possible to notice that for both Configuration 1 and Configuration 2 the failure mode is always cohesive.

5.1.2.2 Fatigue Performance

In this section, the effect of substrate manufacturing method on Double Lap Joints fatigue performance is discussed. In order to assess the influence of material manufacturing on the fatigue performance of DLJs, three levels of maximum load have been investigated, while the stress ratio R is kept constant and equal to 0.1. The frequency is set equal to 10 Hz. For each configuration, in order to obtain a more reliable SN curve, 4 repetitions have been performed for each point.

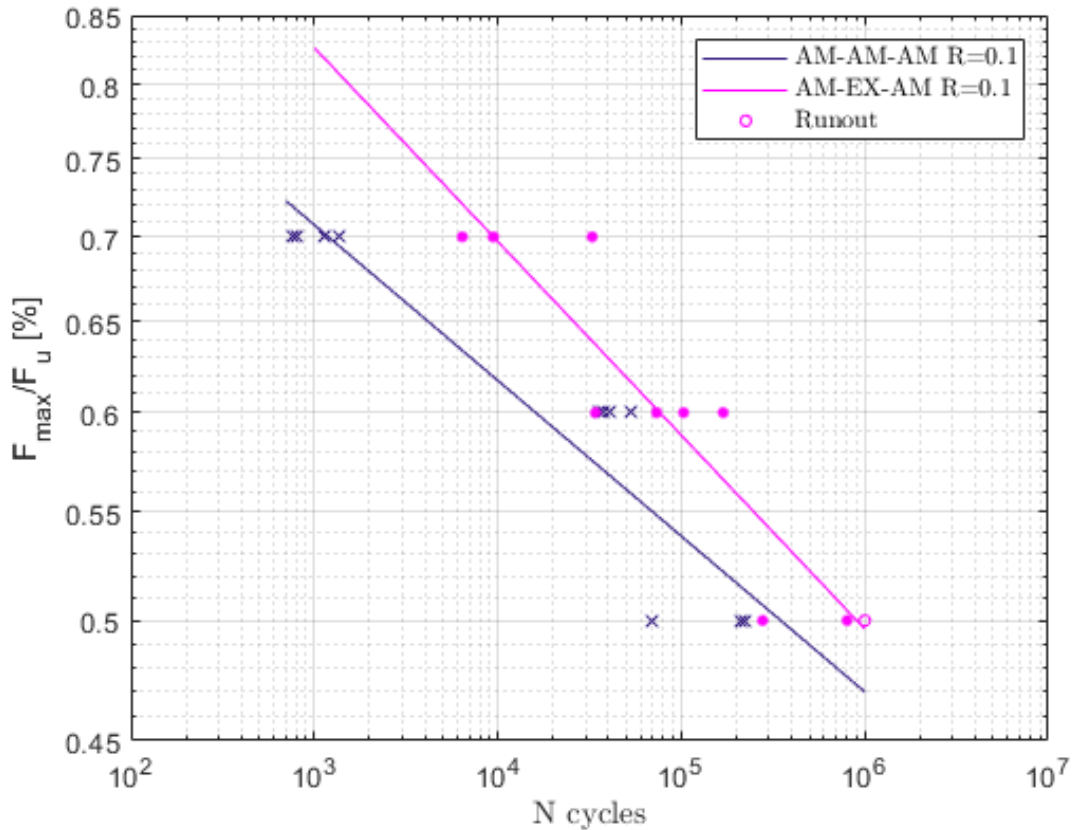


Figure 5.20: Fatigue performance of Double Lap Joints with AM-AM-AM vs. AM-EX-AM substrates – R=0.1

Figure 5.20 shows the maximum load F_{\max} as percentage of the average ultimate load F_u versus the fatigue life N , for both the configurations of Double Lap Joints.

Configuration 2 (AM-EX-AM) shows a better performance. Indeed, when the same maximum load (as percentage of the average ultimate load) is applied, the Double Lap Joints made with 3D printed and extruded substrates have a longer fatigue life. The points represented by an empty circle are runouts points. Runout is a test which is interrupted before it fails. In this research, if a joint survives 10^6 cycles, the MTS machine stops, and the test is interrupted before the failure of the joint. Since the average ultimate load F_u is slightly different for the two configurations, if the percentage is the same, the actual maximum load applied will slightly vary between

the two configurations of DLJs. Therefore, it is useful to plot the alternating load F_a versus the number of cycles.

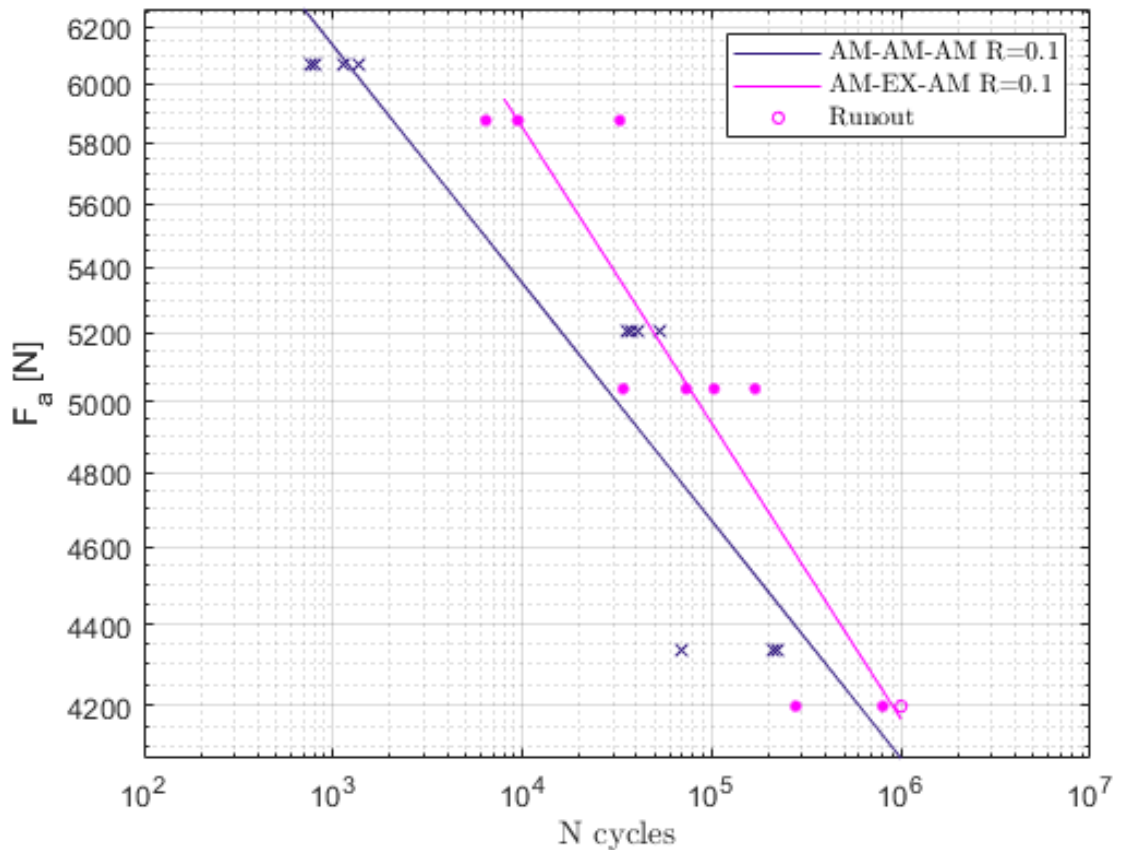


Figure 5.21: Fatigue performance of Double Lap Joints with AM-AM-AM vs. AM-EX-AM substrates – R=0.1

In this case, the outcome does not change. Figure 5.21 shows that, if the same alternating load F_a is applied, Configuration 2 (AM-EX-AM) shows a better performance, since it is able to last more cycles. Figure 5.22 shows the alternating stress S_a versus the number of cycles to failure N , for both the configurations. The alternating stress S_a is obtained dividing the applied alternating load F_a by the total

bonding area A_{tot} . Since in a Double Lap Joint three substrates are bonded together, there are two bonding areas, on both sides of the middle substrate. In Fig.5.22, the adhesive is highlighted with red color.

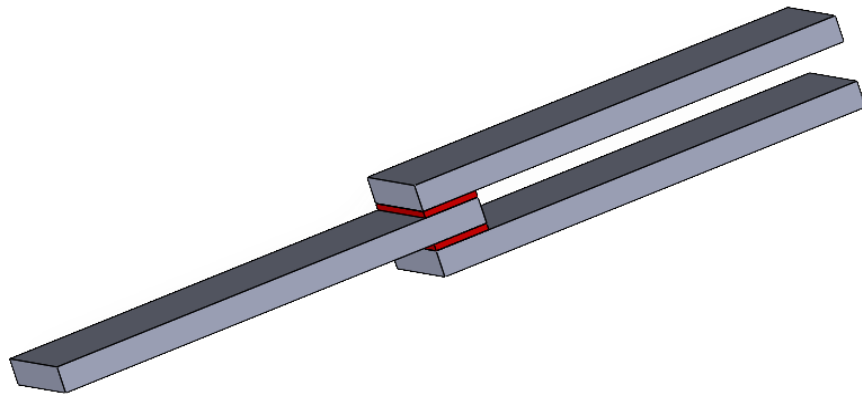


Figure 5.22: 3D representation of a Double Lap Joint

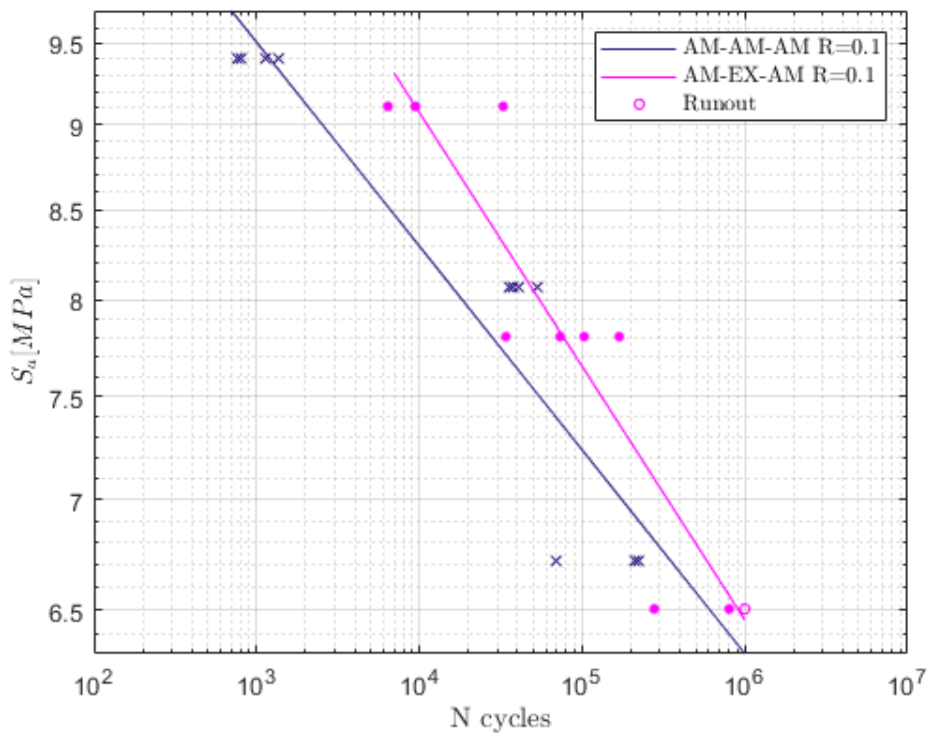


Figure 5.23: SN curves showing the influence of substrate manufacturing on fatigue performance of Double Lap Joints

Both the alternating stress and number of cycles are displayed on logarithmic scales. Looking at the fracture surfaces of the DLJs after the failure, for both Configuration 1 (AM-AM-AM) and Configuration 2 (AM-EX-AM) the failure mode is always cohesive, as Fig.5.24 and Fig.5.25 show. Even when the highest loads are applied it does not switch to adhesive or mixed failure, meaning that the bonding surface has been accurately and correctly prepared. Figures 5.24 and 5.25 show the Fracture Surface of the two configurations. The adhesive layer of the DLJs made only with additive manufactured substrates shows the presence of air bubbles. These latter are probably responsible of the lower fatigue performance of Configuration 1 (AM-AM-AM) with respect to Configuration 2 (AM-EX-AM). This can be due to the different Average Surface Roughness R_a and surface profile.

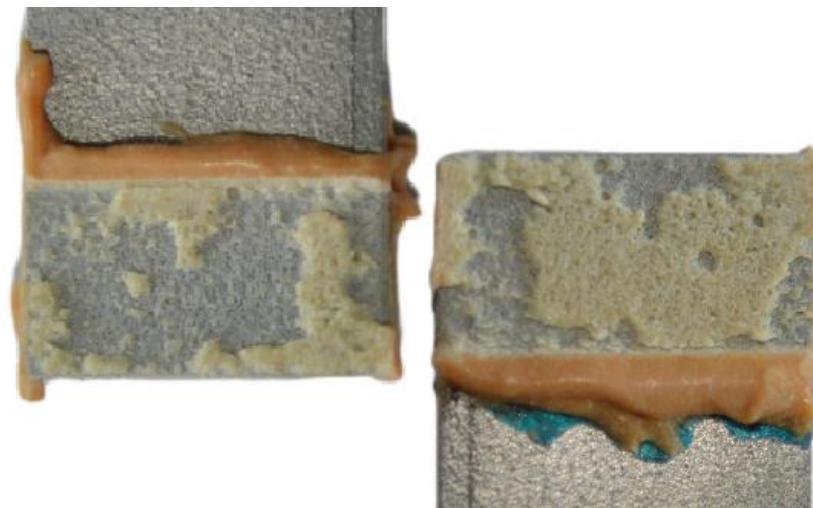


Figure 5.24: Fracture Surface for Configuration 1 (AM-AM-AM)

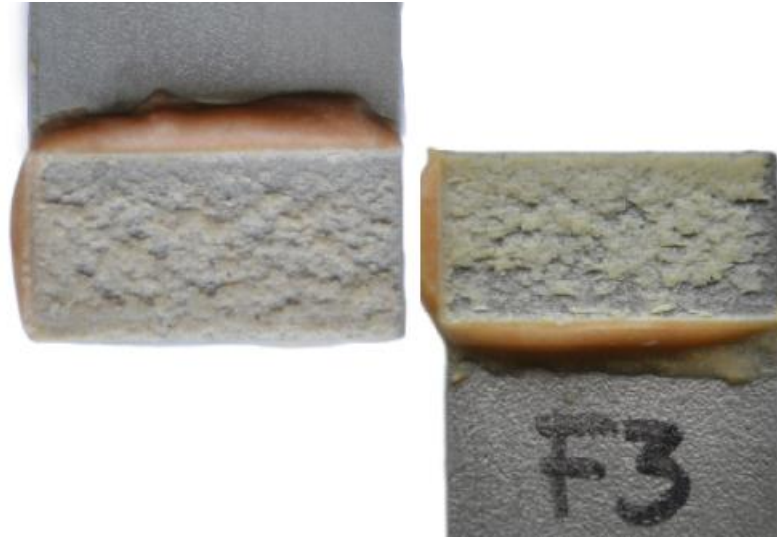


Figure 5.25: Fracture Surface for Configuration 2 (AM-EX-AM)

Using the WYKO NT1100 optical profiler system, it is possible to have a closer look to the surface.

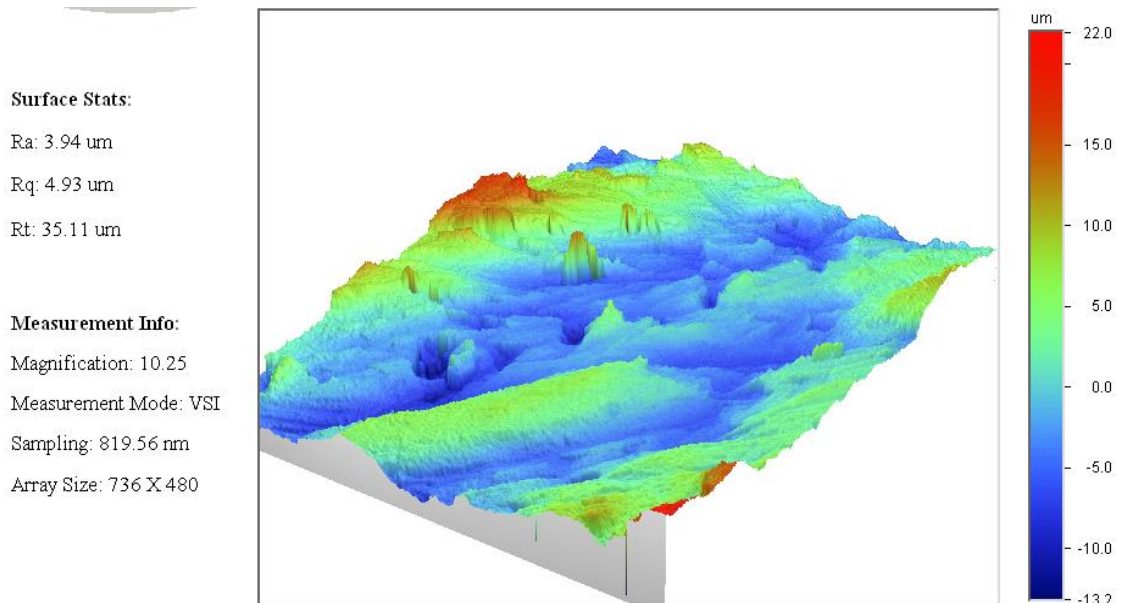


Figure 5.26: 3D surface roughness of an additive manufactured substrate

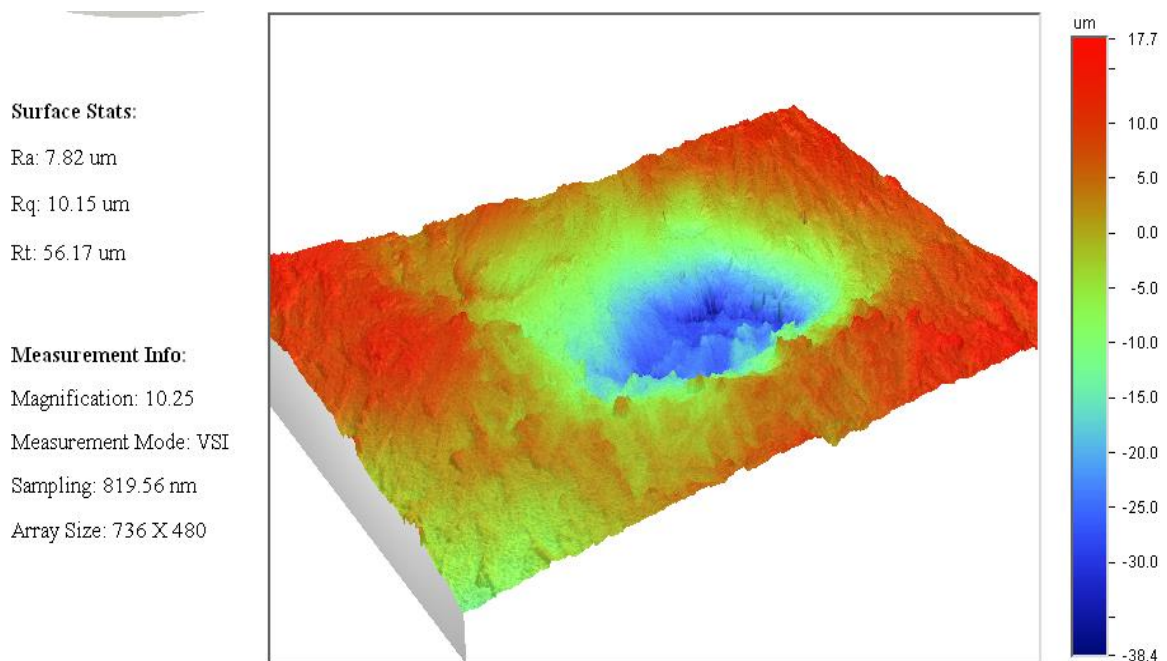


Figure 5.27: Detail of a pore on the additive manufactured surface

Figure 5.26 shows the 3D measurement of the surface of an additive manufactured substrate, after being prepared with the utilization of the wire brush. The Average Surface Roughness R_a is equal to $3.94 \mu\text{m}$ and the surface profile is characterized by the presence of pores. One of these is shown in Fig.5.27.

Figure 5.28 shows the 3D measurement of the surface of an extruded substrate, after being prepared with the utilization of the wire brush. The Average Surface Roughness R_a is equal to $3.33 \mu\text{m}$. Therefore, the difference with respect to the additive manufactured Average Surface Roughness is minor. The surface profile, as Figure 5.28 shows clearly, is characterized by the presence of peaks, instead of pores.

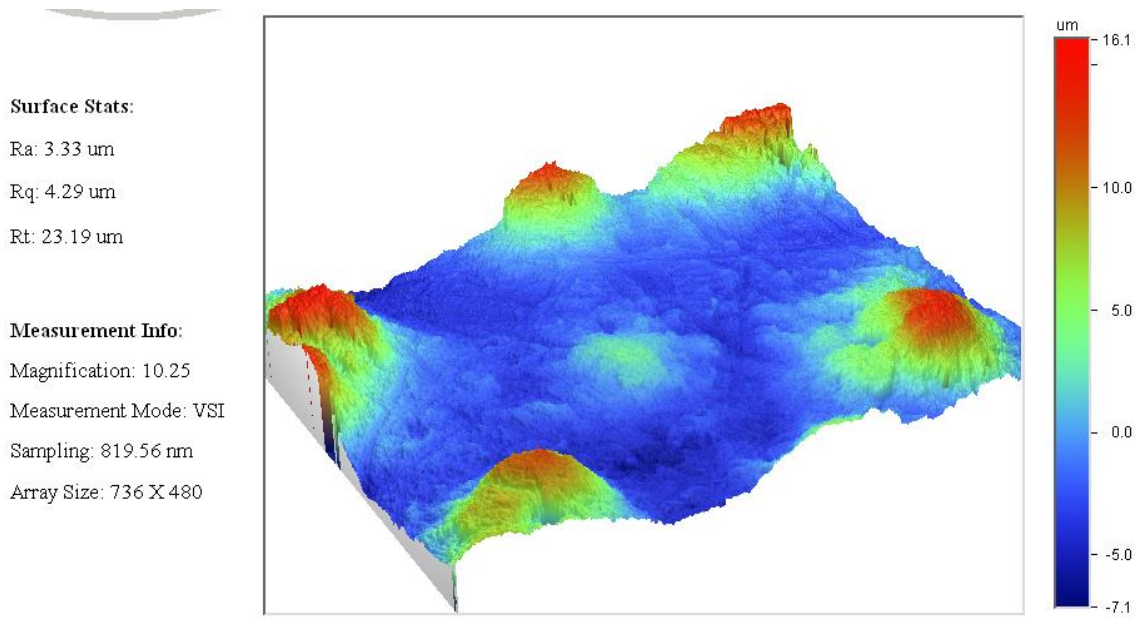


Figure 5.28: 3D surface measurement of an extruded substate

Surface Roughness is a significant variable affecting the mechanical behavior of the joints. Increasing the surface roughness and the asperities of the material can encourage the mechanical interlocking of the adhesive, improving the strength of the joint. This did not happen during the experimental tests performed in this research. Probably, the surface profile of the additive manufactured surface, characterized by the presence of pores, has to be hold accountable of the air trapped inside the adhesive layer, with the adhesive not being able to wet the surface properly. The resulting air gaps lead to a lowering of the joint performance both under static and fatigue loads. Fatigue tests were performed on Double Lap Joints, after adhesive has cured under vacuum conditions inside an autoclave. The aim was to find a method to squeeze the air out of the adhesive layer. Figure 5.29 shows the fracture surface of these joints. The problem was still present and the size of the air bubbles increased.



Figure 5.29: Fracture surface of DLJs cured in autoclave

This is probably due to the fact that the NCA adhesive used to bond the DLJs presents a physical blowing agent inside his composition. Indeed, this adhesive when heat cured show a certain shrinkage, that for standard application is acceptable, but in case of an injection, can represent a problem. In order to compensate the shrinkage, the blowing agent was added to the composition. Applying vacuum, this gas expands more and the air bubbles become bigger.

In order to investigate the effect of the stress ratio R on the fatigue performance of DLJs, additional fatigue tests have been performed using the AM-EX-AM configuration (Configuration 2). For the same stress ratio $R=0.3$, three levels of maximum load have been investigated, for a sample size of 3 replicas of each test.

Figure 5.30 shows the maximum load F_{max} as percentage of the average ultimate load F_u versus the number of cycles to failure N , for two values of Stress Ratio R on the same configuration (AM-EX-AM) of Double Lap Joints. Since the tests are performed on the same configuration of joints, the average ultimate load F_u is the same. Both the load and number of cycles are displayed on logarithmic scales.

When the same maximum load is applied, the higher the stress ratio R the higher the fatigue life. Indeed, if the maximum load F_{max} is the same but the stress ratio R

increases, the alternating load will decrease, leading to a better performance of the joints. The slope of the line interpolating the points is the same.

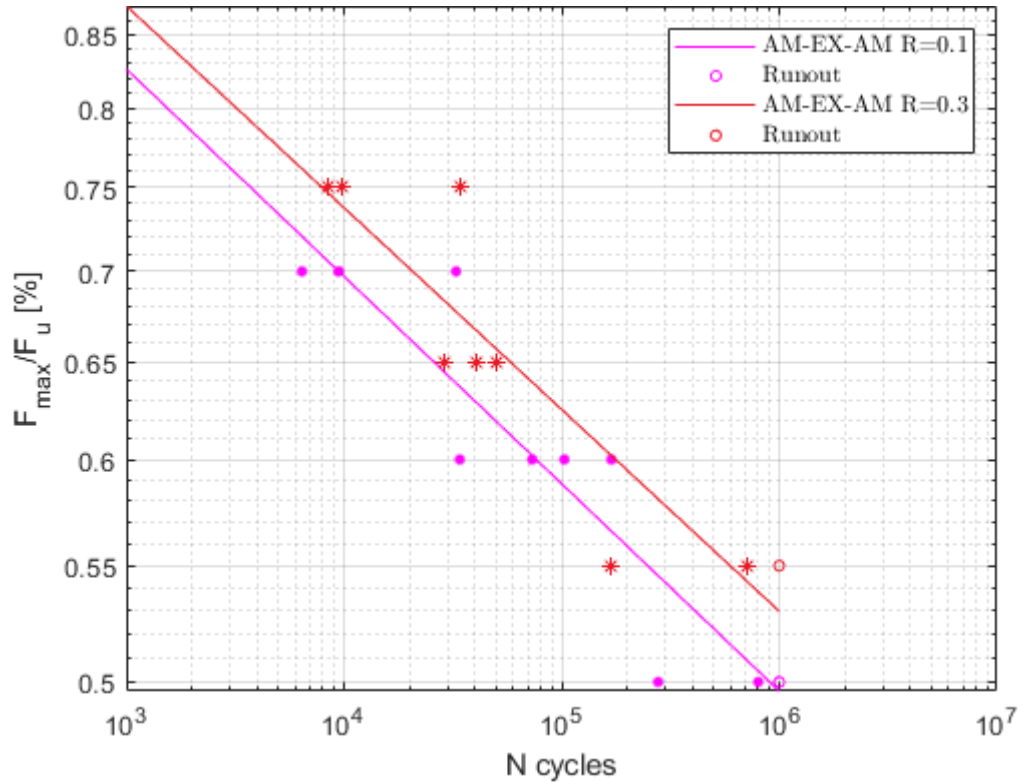


Figure 5.30: Effect of Stress Ratio on fatigue performance of Double Lap Joints

In Figure 5.31, the alternating load F_a versus the number of cycles to failure, for the two values of Stress Ratio R , is shown. Both the load and number of cycles are displayed on logarithmic scales. When the same alternating load is applied, the higher the stress ratio R the lower the fatigue life. Indeed, if the alternating load F_a is the same but the stress ratio R increases, the maximum load will increase, leading to a worse performance of the joints. Figure 5.32 shows the alternating stress S_a versus the number of cycles to failure N , for both the stress ratio R .

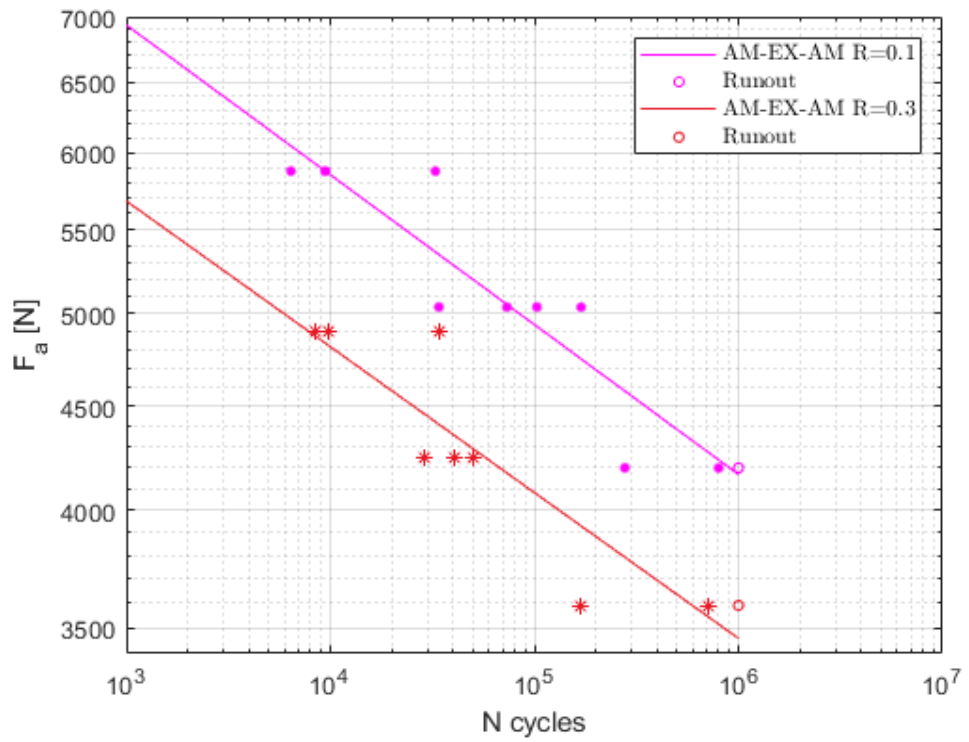


Figure 5.31: Effect of Stress Ratio on fatigue performance of Double Lap Joints

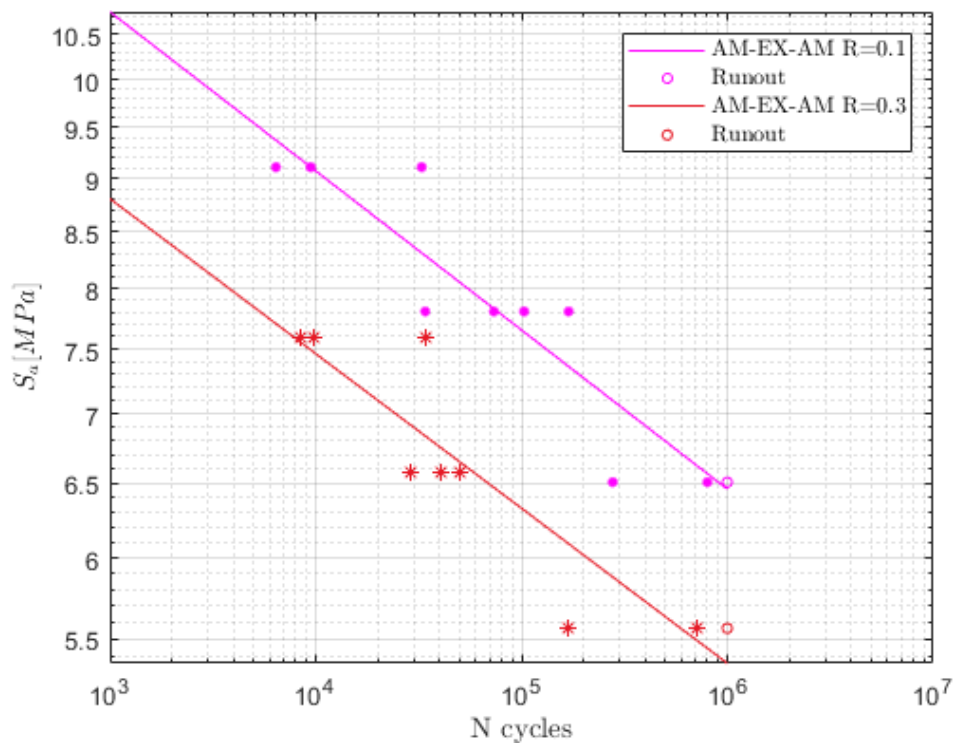


Figure 5.32: SN curves showing the influence of stress ratio on fatigue performance of Double Lap Joints

5.2 Finite element results

5.2.1 Static results

In this section, the FEA results are shown after having characterized the main adhesive parameters. As already explained in Chapter 3, Cohesive Zone Modeling has been used to characterize the NCA single-part epoxy adhesive. Starting from the values found in a previous work [1], the parameters have been tuned in order to fit the experimental static curves.

In Fig.5.33 the mechanical behavior of the DLJs predicted with the FEA can be appreciated. It is possible to observe that:

- Stress distributions are symmetric.
- The stress in the adherends (Von Mises) increases up to 118 MPa until the adhesive gets damaged and starts to lose its load transfer capability.
- No rotations of the adherends are present, since in DLJ we do not have an eccentric load.

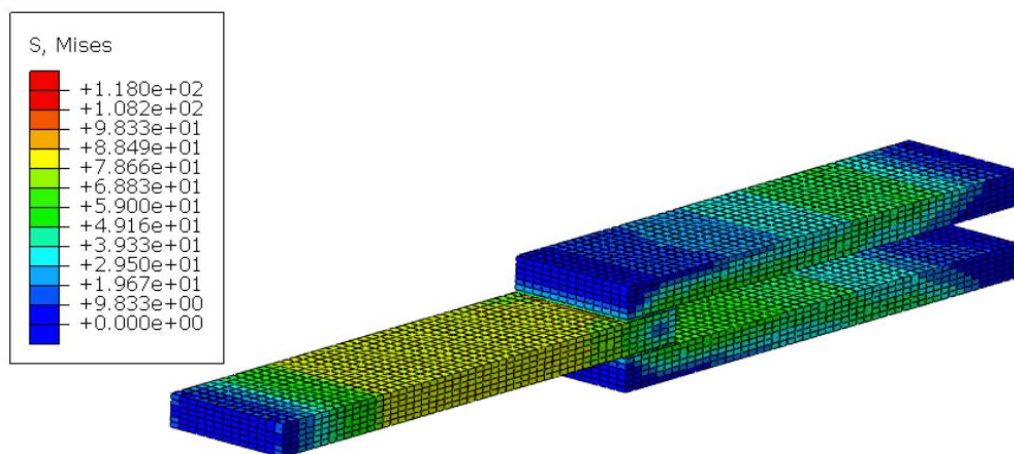


Figure 5.33: Finite Element Analysis: Double Lap Joint Shear Testing

In order to monitor the behavior and the evolution of the adhesive during the test, many parameters can be exploited, such as the Quadratic Nominal Stress Damage Initiation Criterion (QUADSCRT) which allows to understand when the adhesive starts to get damaged, or the Stiffness Degradation (SDEG) which instead allows to understand how far the damage has gone.

In Fig.5.34, QUADSCRT in the adhesive is reported when the load applied is equal to the ultimate load F_u . The adhesive reaches almost uniformly its elastic limit, when the DAMAGE=1. On the overlap ends of the adhesive the zones are more loaded and the complete damage occurs earlier. This is what happens when a proper modeling of the adhesive behavior is performed. Nevertheless, since the considered overlap is really small (12.7 mm), the adhesive layer will more or less degrade uniformly as shown in Fig. 5.35. Figure 5.35 shows that a nearly uniform level of damage exists in the adhesive, as signified by the uniform color.

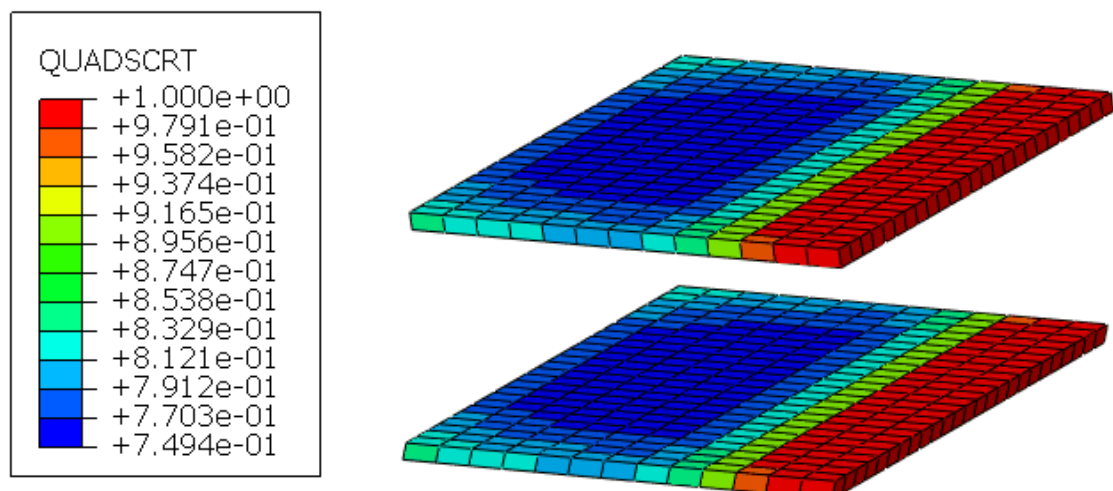


Figure 5.34: Quadratic Nominal Stress Criterion of the Adhesive in the Finite Element Analysis

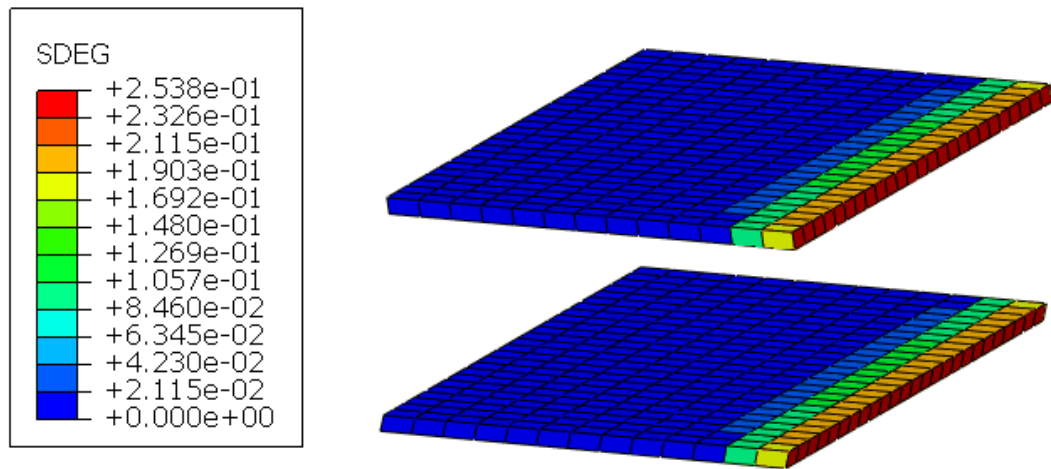


Figure 5.35: Stiffness Degradation of the Adhesive in the Finite Element Analysis

The load displacement curves obtained by FE analysis can be compared with the experimental data. In order to obtain accurate measurements, the adhesive displacement is measured using an extensometer during the static tests. In this way, it is possible to avoid errors due to the measurement of the crosshead displacement. The gauge length is 50mm. A sample placed in the MTS machine with the extensometer is shown in Fig.5.36. The load-displacement curves coming from the experimental tests performed with the extensometer and the load-displacement curve coming from the FE analysis are shown and compared in Fig.5.37. It is possible to appreciate how the numerical curves fit the experimental ones.



Figure 5.36: DLJ placed on the MTS machine with an extensometer

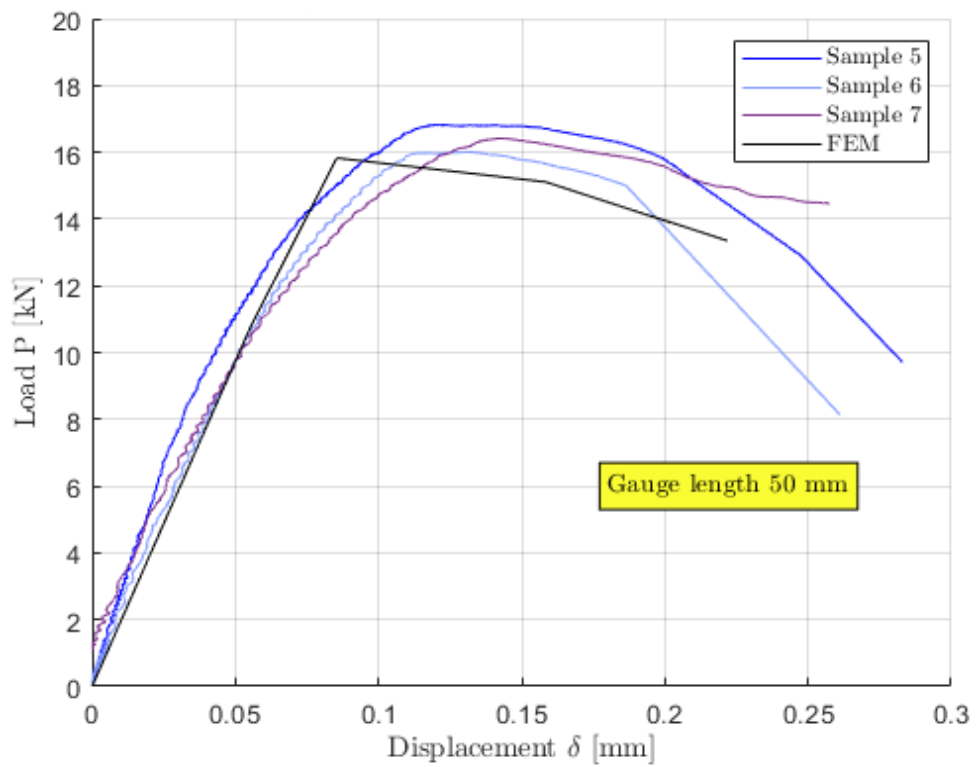


Figure 5.37: Comparison Finite Element Analysis vs. Experimental Tests

The stiffness of the experimental curves slightly changes when the displacement increases, showing a plastic behavior around 10kN. This behavior cannot be fully modelled with a cohesive zone model with a triangular traction-separation law. As a consequence, the numerical stiffness is very close just to the initial values of the experimental curves. The stiffness of the FEM tends to be slightly higher than the real testing (of about 10%). The FEA is able to predict with a good accuracy the ultimate load of the DLJ, based on the data coming from the experimental tests, therefore representing a reliable tool.

5.2.2 Fatigue Performance

One of the main goals of this study is to experimentally characterize the fatigue behavior of the NCA adhesive and to develop methodology to simulate the fatigue behavior of the adhesive. In this section, the results coming from the utilization of the software nCode Design Life are shown and compared with the experimental fatigue results.

The linear elastic model considered 2mm C3D8I elements for the adherends and different mesh sizes and element thickness for the adhesive. Indeed, a sensitivity analysis has been carried on in order to investigate the effect of the increased discretization on the accuracy of the results. To investigate how much the converged solution changes, the following mesh sizes have been considered:

- 2x2mm elements, 0.5mm thick
- 1x1mm elements, 0.5mm thick
- 0.5x0.5mm elements, 0.5mm thick

The element thickness is kept constant and equal to 0.5 mm. Being the adhesive thickness of the joints equal to 0.5 mm, only one layer of linear elastic elements is

needed. Then, to study the effect of the element thickness on the results, the following cases have been considered:

- 0.5x0.5mm elements, 0.5mm thick
- 0.5x0.5mm elements, 0.25mm thick

The mesh size is kept constant and equal to 0.5x0.5mm. In the case of elements 0.25mm thick, two layers of linear elastic elements are needed in order to replace the adhesive.

5.2.2.1 Effect of mesh size

Figure 5.38 compares the nCode Design Life results for different mesh sizes, as compared to the experimental tests performed on AM-AM-AM configuration, with a stress ratio $R=0.1$. Figures 5.39 and 5.40, respectively, compare the results predicted with the results coming from the experimental tests, performed on Configuration 2 (AM-EX-AM) when the stress ratio R is equal to 0.1 and 0.3. From Figures 5.38, 5.39 and 5.40, nCode Design Life simulates fatigue performance with a good accuracy. The software underestimates the fatigue life of the joints in most cases. In one case it overestimates the fatigue life of the joints of about 60 cycles, corresponding to 5%. Also, the results are not too sensitive to mesh size.

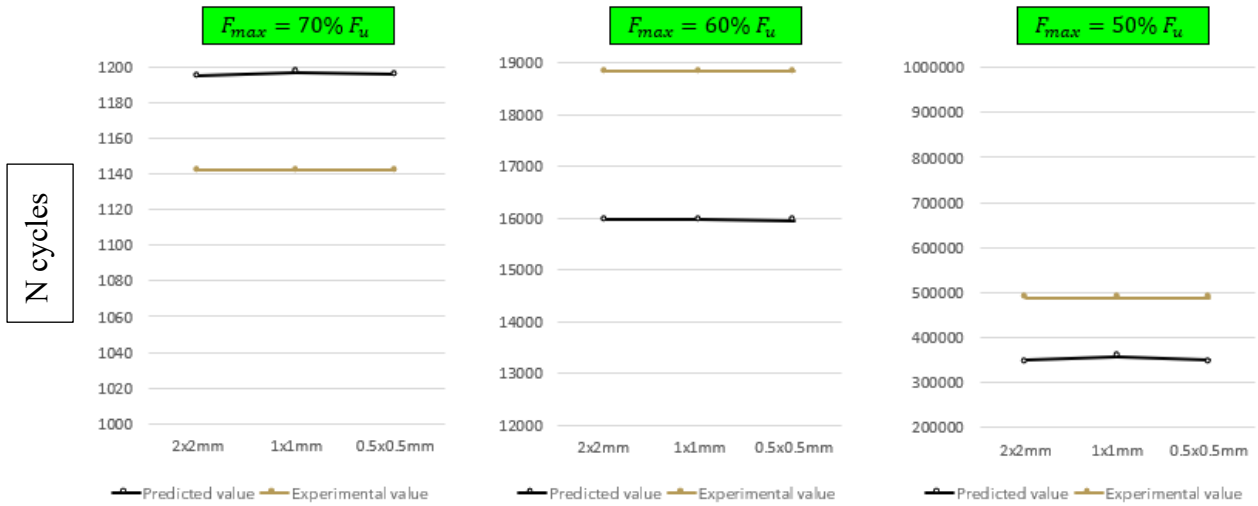


Figure 5.38: Comparison between predicted and experimental values when different maximum loads are applied – AM-AM-AM DLJs (R=0.1)

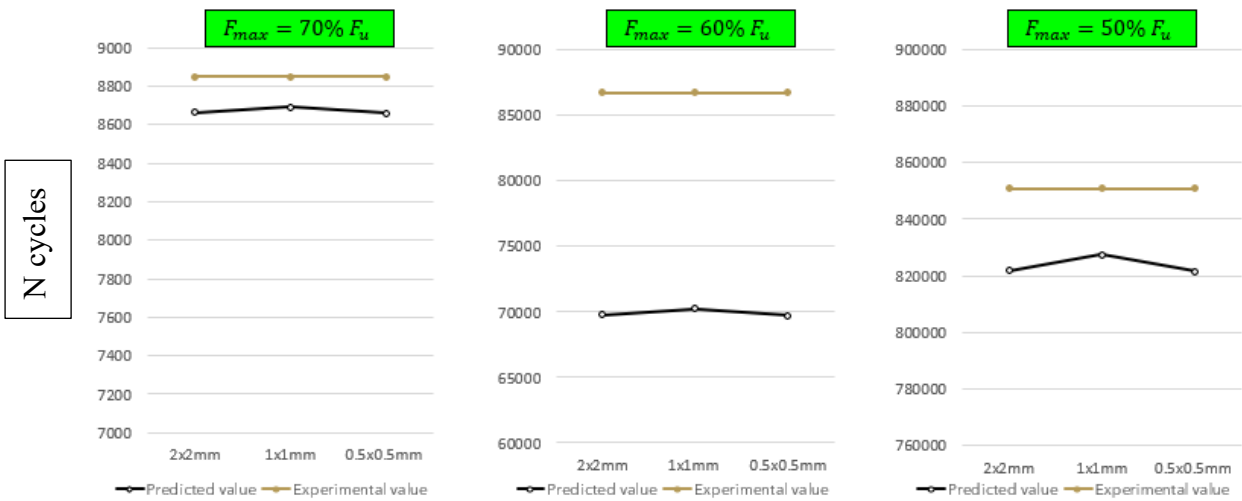


Figure 5.39: Comparison between predicted and experimental values when different maximum loads are applied – AM-EX-AM DLJs (R=0.1)

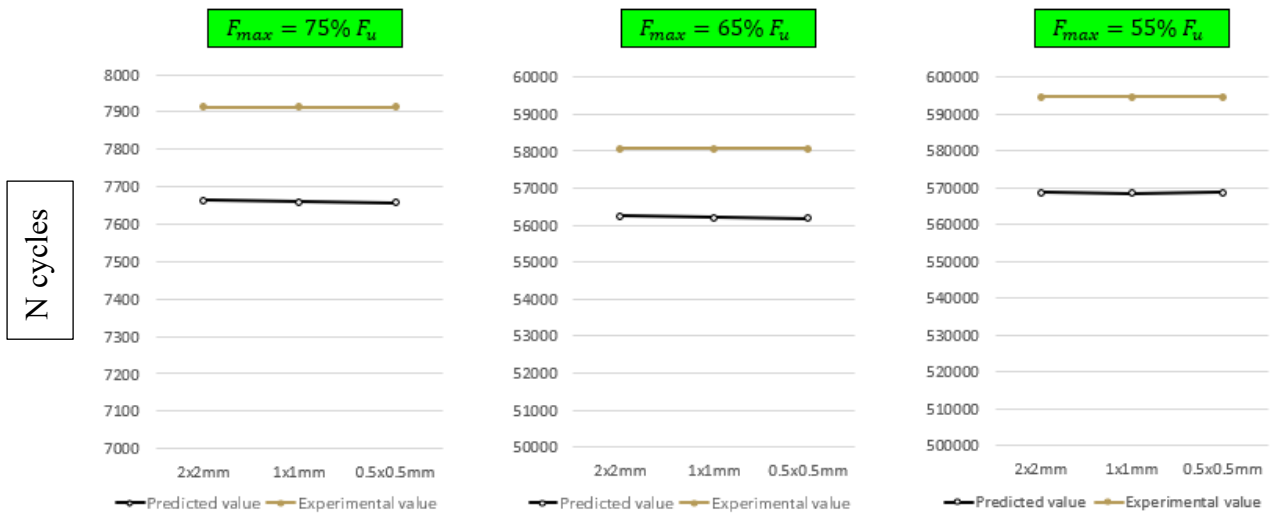


Figure 5.40: Comparison between predicted and experimental values when different maximum loads are applied - AM-EX-AM DLJs (R=0.3)

5.2.2.2 Effect of reducing adhesive thickness

The bar charts in Fig.5.41 compare the results predicted by the software nCode when different adhesive thicknesses are considered with the results coming from the experimental tests, performed on Configuration 1 (AM-AM-AM). The mesh size is fixed and it is equal to 0.5mmx0.5mm. A stress ratio equal to 0.1 is considered.

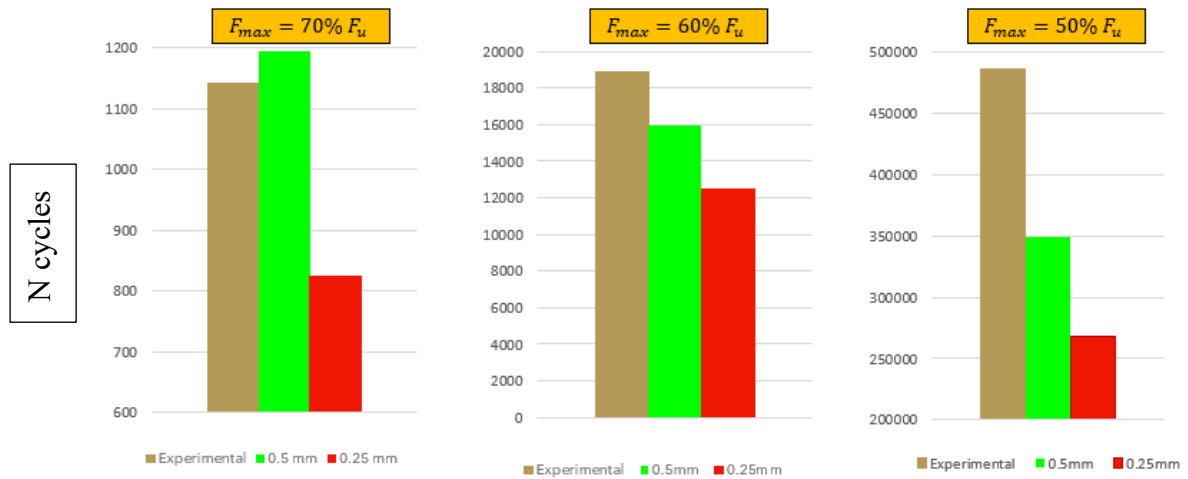


Figure 5.41: Comparison between predicted and experimental values when different maximum loads are applied - AM-AM-AM DLJs (R=0.1)

Figures 5.42 and 5.43, respectively, compare the fatigue life predicted by the software with the results coming from the experimental tests, performed on AM-EX-AM configuration with a stress ratio R=0.1 and R=0.3.

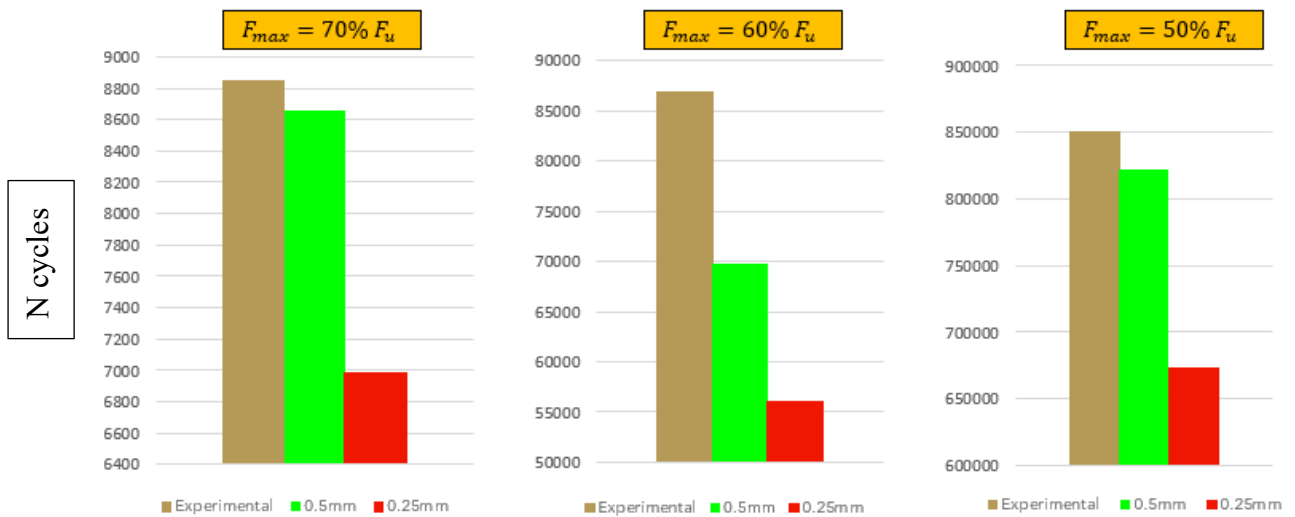


Figure 5.42: Comparison between predicted and experimental values when different maximum loads are applied - AM-EX-AM DLJs (R=0.1)

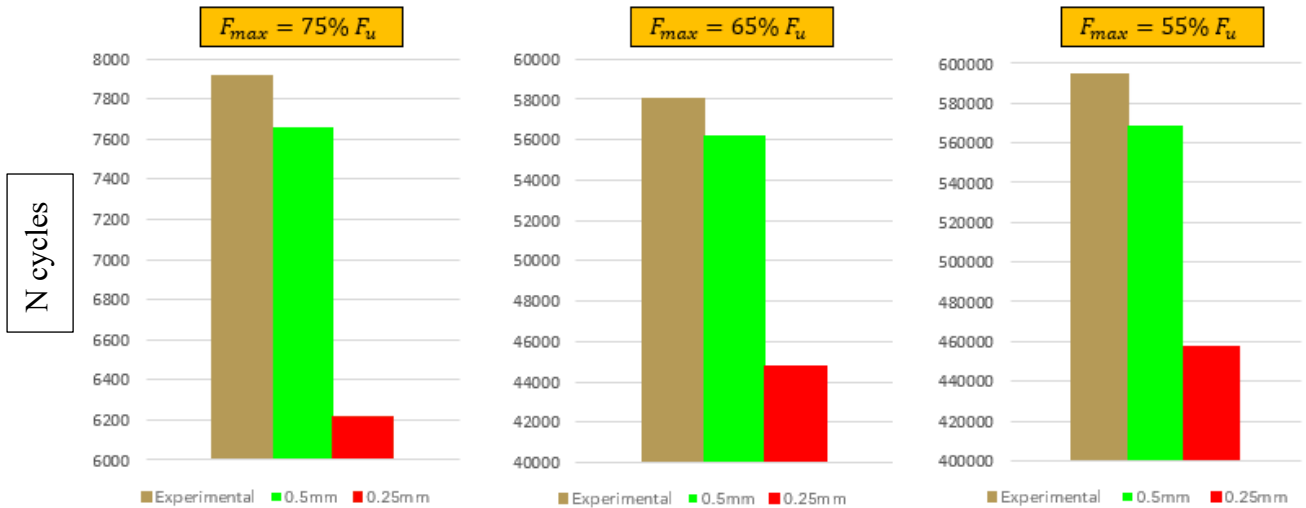


Figure 5.43: Comparison between predicted and experimental values when different maximum loads are applied - AM-EX-AM DLJs (R=0.3)

Figures 5.41, 5.42 and 5.43 show that fatigue life predicted by the software is sensitive to the thickness of the elements used for the adhesive. Reducing the element thickness decreases the accuracy of the prediction. Using only one element (0.5mm thick) in the adhesive layer, the estimated life is closer to the experimental reference value. In all the cases, the methodology used to predict fatigue life underestimates the fatigue life of the adhesively bonded joints.

CHAPTER SIX CONCLUSIONS

In this study, the effect of substrate manufacturing method on fatigue life of adhesively bonded joints is assessed using analytical and experimental methods. Experimental results showed a significantly improved fatigue performance of adhesively bonded single lap joint with 3D printed stainless steel substrates (AM-AM) as compared to wrought substrates (WR-WR). Observed increase of the Surface Roughness of 3D printed (AM) substrates provided stronger adhesion that led to longer fatigue life of the joints. This does not happen for the aluminum double lap joints, where the 3D printed substrates lowered the fatigue performance, due to the formation of large pores (air bubbles) inside the 3D-printed adhesive layer. Change of Surface Roughness on wrought Single Lap Joints does not lead to significant differences. At lower loads (higher cycles) a switch in the failure mode is observed for the samples with lower surface roughness. Concerning the effect of mean load, the trend remains the same when switching from a value of mean load to another one.

CZM parameters for the FEA model were finely tuned using the static experimental data. A methodology to predict fatigue life has been developed, using the software nCode Design Life, that predicted joint fatigue life with a good accuracy.

CONTINUATION STUDIES

Future work could include adhesive characterization under high strain rates from impact loading, as well further the investigation of the effect of surface treatment on the static and dynamic joint performance of adhesively bonded joints.

REFERENCES

- [1] D. Nappi, 2021, “Effect of key design variables on adhesively bonded joints with additive manufacturing substrates”, Master’s Thesis, Oakland University.
- [2] Lucas F.M. da Silva, Paulo J.C. das Neves, R.D. Adams, J.K. Spelt, 2009, International Journal of Adhesion & Adhesives, “Analytical Models of Adhesively Bonded Joints – Part I: Literature Survey”, V.29, pp. 319-330.
- [3] Lucas F.M. da Silva, Paulo J.C. das Neves, R.D. Adams, A. Wang, J.K. Spelt, 2009, International Journal of Adhesion & Adhesives, “Analytical Models of Adhesively Bonded Joints – Part II: Comparative Study”, V.29, pp. 331-341.
- [4] L. Goglio, M. Rossetto, 2011, International Journal of Adhesion & Adhesives, “Precision of the one-dimensional solutions for bonded double lap joints”, V.31, pp.301-314.
- [5] A. M. Pereira, P. N. B. Reis & J. A. M. Ferreira, 2017, The Journal of Adhesion, “Effect of the mean stress on the fatigue behaviour of single lap joints”, 93:6, pp.504-513.
- [6] H. Khoramishad, A.D. Crocombe, K.B. Katnam, I.A. Ashcroft, 2010, International Journal of Adhesion & Adhesives, “A generalized damage model for constant amplitude fatigue loading of adhesively bonded joints”, V.30, pp. 513-521.
- [7] M.F.S.F. De Moura, J.P.M Gonçalves, 2014, International Journal of Solids and Structures, “Cohesive zone model for high-cycle fatigue of composite bonded joints under mixed-mode I+II loading”, V.51, pp.1123,1131.
- [8] R.D. Adams, N.A. Peppiat, 1974, The Journal of Strain Analysis for Engineering Design, “Stress Analysis of Adhesive-Bonded Lap Joints”,V.9, pp.185-196.
- [9] Mohammed, K.M. Liechti, 2000, J Mech Phys Solids, “Cohesive zone modeling of crack nucleation at bimaterial corners”,V.48, pp.735–64.
- [10] P. Rahulkumar, A. Jagota, S.J. Bennison, S. Saigal, 2000, Int J Solids Struct, “Cohesive element modeling of viscoelastic fracture: application to peel testing of polymers”, V.37, pp.1873–97.
- [11] N. Chandra, H. Li, C. Shet, H. Ghonem, 2002, Int J Solids Struct, “Some issues in the application of cohesive zone models for metal–ceramic interfaces”, V.39, pp.2827–55.

REFERENCES – Continued

- [12] J.G. Rots, 1986, Elsevier Science Publishers, “Strain-softening analysis of concrete fracture specimens”, p. 137–48
- [13] M. Frascio, L. Bergonzi, M. Jilich, F. Moroni, M. Avalle, A. Pirondi, M. Monti, M. Vettori, 2019, Acta Polytechnica CTU Proceedings, “Additive Manufacturing Process Parameter Influence on Mechanical Strength of Adhesive Joints, Preliminary Activities”, V.25, pp.41-47.
- [14] M. Frascio, C. Mandolino L. Bergonzi, M. Jilich, F. Moroni, M. Avalle, A. Pirondi, M. Monti, M. Vettori, 2021, International Journal of Adhesion & Adhesives, “Appraisal of surface preparation in adhesive bonding of additive manufactured substrates”, V.106, pp.1-9.
- [15] A.D. Crocombe, G. Richardson, 1999, International Journal of Adhesion & Adhesives, “Assessing stress state and mean load effects on the fatigue response of adhesively bonded joints”, V.19, pp.19-27.
- [16] H. Khoramishad, A.D. Crocombe, K.B. Katnam, I.A. Ashcroft, 2010, International Journal of Adhesion & Adhesives, “Predicting fatigue damage in adhesively bonded joints using cohesive zone model”, V.32, pp. 1146-1158.